Atmos. Chem. Phys., 16, 9361–9379, 2016
www.atmos-chem-phys.net/16/9361/2016/
doi:10.5194/acp-16-9361-2016

Atmospheric Chemistry and Physics Open Access EGU

Influence of seed aerosol surface area and oxidation rate on vapor wall deposition and SOA mass yields: a case study with α-pinene ozonolysis

Theodora Nah[1], Renee C. McVay[2], Xuan Zhang[3,a], Christopher M. Boyd[1], John H. Seinfeld[2,3], and Nga L. Ng[1,4]

[1]School of Chemical and Biomolecular Engineering, Georgia Institute of Technology, Atlanta, GA, USA
[2]Division of Chemistry and Chemical Engineering, California Institute of Technology, Pasadena, CA, USA
[3]Division of Engineering and Applied Science, California Institute of Technology, Pasadena, CA, USA
[4]School of Earth and Atmospheric Sciences, Georgia Institute of Technology, Atlanta, GA, USA
[a]now at: Center for Aerosol and Cloud Chemistry, Aerodyne Research, Billerica, MA, USA

Correspondence to: Nga L. Ng (ng@chbe.gatech.edu)

Received: 29 March 2016 – Published in Atmos. Chem. Phys. Discuss.: 4 April 2016
Revised: 6 July 2016 – Accepted: 9 July 2016 – Published: 28 July 2016

Abstract. Laboratory chambers, invaluable in atmospheric chemistry and aerosol formation studies, are subject to particle and vapor wall deposition, processes that need to be accounted for in order to accurately determine secondary organic aerosol (SOA) mass yields. Although particle wall deposition is reasonably well understood and usually accounted for, vapor wall deposition is less so. The effects of vapor wall deposition on SOA mass yields in chamber experiments can be constrained experimentally by increasing the seed aerosol surface area to promote the preferential condensation of SOA-forming vapors onto seed aerosol. Here, we study the influence of seed aerosol surface area and oxidation rate on SOA formation in α-pinene ozonolysis. The observations are analyzed using a coupled vapor–particle dynamics model to interpret the roles of gas–particle partitioning (quasi-equilibrium vs. kinetically limited SOA growth) and α-pinene oxidation rate in influencing vapor wall deposition. We find that the SOA growth rate and mass yields are independent of seed surface area within the range of seed surface area concentrations used in this study. This behavior arises when the condensation of SOA-forming vapors is dominated by quasi-equilibrium growth. Faster α-pinene oxidation rates and higher SOA mass yields are observed at increasing O_3 concentrations for the same initial α-pinene concentration. When the α-pinene oxidation rate increases relative to vapor wall deposition, rapidly produced SOA-forming oxidation products condense more readily onto seed aerosol particles, resulting in higher SOA mass yields. Our results indicate that the extent to which vapor wall deposition affects SOA mass yields depends on the particular volatility organic compound system and can be mitigated through the use of excess oxidant concentrations.

1 Introduction

Secondary organic aerosol (SOA), formed from the oxidation of volatile and intermediate-volatility organic compounds (VOCs and IVOCs), contributes a significant fraction of the global organic aerosol burden (Kanakidou et al., 2005; Hallquist et al., 2009; Tsigaridis et al., 2014). SOA formation studies, which are typically conducted in laboratory chambers in the presence of seed aerosol particles, provide fundamental data that can be used to predict the rate of atmospheric SOA formation. An essential parameter of interest in laboratory chamber studies is the SOA mass yield (Y), which is defined as the ratio of mass concentration of SOA formed to mass concentration of parent hydrocarbon reacted ($(\Delta\mathrm{HC})$, $Y = \Delta M_o/\Delta\mathrm{HC}$; Odum et al., 1996, 1997a, b). The measured SOA mass yields can subsequently be applied in atmospheric models to predict regional and global organic aerosol burdens. In order to obtain accurate SOA mass yields from the evolving aerosol size distribution in chamber experiments, the loss of both particles and vapors to the chamber

walls needs to be accurately accounted for (Crump and Seinfeld, 1981; McMurry and Grosjean, 1985; McMurry and Rader, 1985; Cocker et al., 2001a; Weitkamp et al., 2007; Pierce et al., 2008; Hildebrandt et al., 2009; Loza et al., 2010, 2012; Matsunaga and Ziemann, 2010; Kokkola et al., 2014; McVay et al., 2014; Yeh and Ziemann, 2014, 2015; Zhang et al., 2014, 2015a; La et al., 2016; Ye et al., 2016).

The mechanisms by which particles in chambers deposit on chamber walls are reasonably well understood. Particles are transported to the boundary layer on the chamber walls via diffusion, gravitational settling, and electrostatic forces (Crump and Seinfeld, 1981; McMurry and Grosjean, 1985; McMurry and Rader, 1985; Pierce et al., 2008). The rate at which particles are transported to the edge of the boundary layer is dictated primarily by mixing conditions in the chamber. An effective approach for characterizing particle wall loss involves measuring the size-dependent wall loss rates of polydisperse inert seed aerosol (e.g., ammonium sulfate particles) injected into the chamber during seed-only experiments (Keywood et al., 2004; Pierce et al., 2008). The observed particle number concentration decay in each size bin is then fitted to a first-order exponential decay from which the first-order wall loss coefficients are determined as a function of particle size. These wall loss coefficients are subsequently used to correct for size-dependent particle wall loss in actual SOA formation experiments. Determination of particle wall loss coefficients may be complicated if coagulation is significant. Particle dynamics models can be used to correct particle wall loss coefficients for coagulation.

Vapor wall deposition mechanisms in chambers are not as well understood or accounted for as those for particles. The degree to which SOA-forming vapors deposit onto chamber walls is governed by the rate at which these gas-phase organic molecules are transported to the walls, the strength of adherence of the organic molecule to the wall, and the extent of reversible vapor–wall partitioning (Loza et al., 2010; Matsunaga and Ziemann, 2010; Zhang et al., 2015a). For example, Loza et al. (2010) showed that the loss of 2,3-epoxy-1,4-butanediol, an isoprene oxidation product analogue, to walls in the Caltech chamber was essentially irreversible on short timescales but became reversible on longer timescales. In contrast, glyoxal, a common isoprene oxidation product, exhibited reversible vapor–wall partitioning over all timescales. Recent studies show that SOA mass yields measured in chamber experiments can be significantly underestimated due to wall deposition of SOA-forming vapors that would otherwise contribute to SOA growth (McVay et al., 2014; Zhang et al., 2014; La et al., 2016). Zhang et al. (2014) found that chamber-derived SOA mass yields from toluene photooxidation may be underestimated by as much as a factor of 4 as a result of vapor wall loss. Consequently, the use of underestimated chamber-derived SOA mass yields in atmospheric models will lead to the underprediction of ambient SOA mass concentrations (Cappa et al., 2016).

For the toluene photooxidation system, Zhang et al. (2014) showed that the measured SOA mass yields increased with increasing seed aerosol surface area, demonstrating that increasing the seed-to-chamber surface area ratio promoted the condensation of SOA-forming vapors onto seed aerosol particles. However, increasing the seed aerosol surface area to promote condensation of SOA-forming vapors onto seed aerosol particles may not be effective in all VOC oxidation systems. A modeling study by McVay et al. (2014) showed that the SOA mass yield depends on seed aerosol surface area only in cases where the condensation of SOA-forming vapors onto seed aerosol particles is kinetically limited (i.e., the timescale for gas–particle equilibrium is competitive with or greater than the timescale for reaction and vapor wall deposition). In addition to the seed aerosol surface area, VOC oxidation rate may also play an important role in the effect of vapor wall loss on SOA formation. Ng et al. (2007) showed that the SOA mass yields from *m*-xylene photooxidation are dependent on the oxidation rate, with higher OH concentrations (and hence faster oxidation rates) resulting in higher SOA mass yields. It was suggested that the "oxidation rate effect" could arise as a result of competition between growing particles and chamber walls for condensable VOC oxidation products (Ng et al., 2007). However, McVay et al. (2016) reported similar SOA growth at low and high OH concentrations in α-pinene photooxidation. Taken together, these studies show the importance of understanding how gas–particle partitioning and VOC oxidation rate impact vapor wall deposition and SOA mass yields in laboratory chamber experiments.

In this study, we examine the influence of seed aerosol surface area and oxidation rate on SOA formation in α-pinene ozonolysis chamber experiments. α-pinene is the most abundant monoterpene, with global emissions estimated to be $\sim 66\,\mathrm{Tg\,yr^{-1}}$ (Guenther et al., 2012). Ozonolysis is the major atmospheric oxidation pathway of α-pinene, and is estimated to account for reaction of $\sim 46\,\%$ of emitted α-pinene (Griffin et al., 1999; Capouet et al., 2008). α-pinene ozonolysis, a major source of atmospheric SOA on both regional and global scales (Kanakidou et al., 2005; Hallquist et al., 2009; Carlton et al., 2010; Pye et al., 2010), has been the subject of numerous studies (Hoffmann et al., 1997; Griffin et al., 1999; Cocker et al., 2001b; Gao et al., 2004; Presto et al., 2005; Presto and Donahue, 2006; Pathak et al., 2007a, b; Song et al., 2007; Shilling et al., 2008; Henry et al., 2012; Ehn et al., 2014; Kristensen et al., 2014; Zhang et al., 2015b). Here, we measure the α-pinene SOA mass yield as a function of seed aerosol surface area concentration (0 to $3000\,\mu\mathrm{m^2\,cm^{-3}}$) and O_3 mixing ratio (100 vs. 500 ppb). These results are analyzed using a coupled vapor–particle dynamics model to evaluate the roles of gas–particle partitioning and VOC oxidation rate in influencing vapor wall deposition effects on the measured SOA mass yields.

Table 1. Experimental conditions and results for the α-pinene ozonolysis experiments.

Experiment	Initial seed surface area ($\mu m^2\ cm^{-3}$)	Initial [α-pinene][a] ($\mu g\ m^{-3}$)	ΔM_o[b] ($\mu g\ m^{-3}$)	SOA mass yield[c] (%)
100 ppb O_3 nucleation	0	290.2 ± 23.2	62.0 ± 1.2[d]	22.6 ± 1.9
100 ppb O_3 low AS	1130	280.5 ± 22.4	63.0 ± 0.8[d]	23.3 ± 1.9
100 ppb O_3 high AS	2700	238.7 ± 19.1	50.6 ± 1.6[d]	23.3 ± 1.9
500 ppb O_3 nucleation	0	274.4 ± 21.9	87.3 ± 0.3[e]	31.8 ± 2.5
500 ppb O_3 low AS	1300	264.9 ± 21.2	75.7 ± 0.6[e]	28.6 ± 2.3
500 ppb O_3 high AS	2720	236.1 ± 18.9	66.3 ± 1.9[e]	28.1 ± 2.4

[a] Concentration of α-pinene injected into the chamber. All the α-pinene reacted in the 500 ppb O_3 experiments, but not the 100 ppb O_3 experiments. [b] Uncertainties in the peak SOA mass concentration (ΔM_o) are calculated from 1 standard deviation of the aerosol volume as measured by the scanning mobility particle sizer. [c] SOA mass yields at peak SOA growth are reported. [d] The SOA mass concentration is calculated using the density = $1.39\ g\ cm^{-3}$ obtained from the 100 ppb O_3 nucleation experiment. [e] The SOA mass concentration is calculated using the density = $1.37\ g\ cm^{-3}$ obtained from the 500 ppb O_3 nucleation experiment.

2 Experimental

2.1 Dark α-pinene ozonolysis experiments

Experiments were conducted in the Georgia Tech Environmental Chamber (GTEC) facility. Details of the dual-chamber facility are provided elsewhere (Boyd et al., 2015). Only one FEP Teflon chamber (volume $13\ m^3$) was used for the entirety of this study. Before each experiment, the chamber was flushed with dried, purified air for at least 36 h until the aerosol number concentration was $< 30\ cm^{-3}$. All experiments were conducted under dry conditions (< 5 % RH) at room temperature (25 °C). NO_x mixing ratios in these experiments were < 1 ppb. Experimental conditions are summarized in Table 1.

First, 22 ppm of cyclohexane (Sigma Aldrich, ≥ 99.9 %) was injected into the chamber to act as an OH scavenger (∼ 440 times the initial α-pinene concentration). Based on the concentrations of cyclohexane and α-pinene injected into the chamber, the reaction rate of OH with cyclohexane is ∼ 60 times greater than that with α-pinene. After the cyclohexane concentration had stabilized in the chamber for 30 min, a known concentration (∼ 50 ppb in all experiments) of α-pinene (Sigma Aldrich, > 99 %) was injected into the chamber, followed by inorganic seed aerosol via atomization of an aqueous ammonium sulfate (AS) solution (in seeded experiments). To vary the seed aerosol surface area, different concentrations of AS solutions were used to generate seed aerosol particles in the seeded experiments. In the "low-AS" experiments, a 0.015 M AS solution was used to generate seed particles, and the resulting initial total AS seed surface area concentration was $\sim 1000\ \mu m^2\ cm^{-3}$. In the "high-AS" experiments, a 0.05 M AS solution was used to generate seed aerosol particles, and the resulting initial total AS seed surface area concentration was $\sim 3000\ \mu m^2\ cm^{-3}$. In selected experiments, no seed aerosol particles were introduced into the chamber and SOA was formed via nucleation. After the seed aerosol concentration in the chamber stabilized, O_3 (100 or 500 ppb), which was generated by passing purified air into a photochemical cell (Jelight 610), was introduced into the chamber. The start of O_3 injection into the chamber marked the beginning of the reaction (i.e., reaction time = 0 min). The injected α-pinene : O_3 molar ratio was approximately 1 : 2 and 1 : 10 in the 100 and 500 ppb O_3 experiments, respectively. O_3 was injected into the chamber for 13.5 and 54.25 min in the 100 and 500 ppb O_3 experiments, respectively, to achieve the desired O_3 concentrations. Approximately 11 and 98 % of the initial α-pinene had reacted when O_3 injection was completed in the 100 and 500 ppb O_3 experiments, respectively. In the GTEC chamber, α-pinene closest to the O_3 injection port likely reacted first in the α-pinene ozonolysis experiments. The O_3 injection times were established in separate experiments in which only O_3 was injected into the chamber. Based on the O_3 time series traces in the O_3-only experiments, the O_3 mixing timescale was estimated to be ∼ 12 min for all experiments.

The α-pinene and O_3 concentrations were measured by a gas chromatograph–flame ionization detector (GC-FID, Agilent 7890A) and O_3 monitor (Teledyne T400), respectively. GC-FID measurements were taken 12 min apart. A high-resolution time-of-flight aerosol mass spectrometer (HR-ToF-AMS, Aerodyne Research Inc.) was used to measure the aerosol elemental composition (DeCarlo et al., 2006; Canagaratna et al., 2015). Details on the operation of the HR-ToF-AMS and its data analysis are described elsewhere (Canagaratna et al., 2015). Aerosol size distributions, number and volume concentrations were measured by a scanning mobility particle sizer (SMPS, TSI), which consists of a differential mobility analyzer (DMA, TSI 3081) and a condensation particle counter (CPC, TSI 3775). For nucleation and low-AS experiments, the measured aerosol size range was set to 14 to 686 nm diameter. For high-AS experiments, the measured aerosol size range was set to 17 to 983 nm. Prior checks were made to confirm that no particles larger than 686 nm were detected in the nucleation and low-AS experiments. The SOA mass concentrations reported in this study were measured us-

ing the SMPS. The SOA density was calculated from the ratio of the aerosol size distributions measured by the HR-ToF-AMS and the SMPS during nucleation experiments (DeCarlo et al., 2004; Bahreini et al., 2005).

2.2 Particle wall deposition correction

Particle wall deposition needs to be accounted for to determine the SOA mass concentration in the chamber. Two limiting assumptions have traditionally been made regarding interactions between particles deposited on the chamber walls and suspended vapors when accounting for particle wall loss in the computation of SOA mass yields (Weitkamp et al., 2007; Hildebrandt et al., 2009; Loza et al., 2012; Zhang et al., 2014). The first case assumes that particles deposited on the walls cease to interact with suspended vapors, and therefore the SOA mass present on these deposited particles does not change after deposition (Loza et al., 2012; Zhang et al., 2014). Adding the SOA mass present on these deposited particles to that present on the suspended particles provides a lower bound of the total SOA mass concentration. In the second case, it is assumed that particles deposited on the walls continue to interact with suspended vapors as if these particles had remained suspended, and therefore the SOA mass present on these deposited particles increases at the same rate as those suspended (Hildebrandt et al., 2009; Weitkamp et al., 2007). Thus, this case provides an upper bound of the total SOA mass concentration due to the additional uptake of suspended vapors to wall-deposited particles. However, it must be kept in mind that the calculated SOA mass concentration can be underestimated even in the upper bound case since the calculation accounts neither for differences in the vapor–particle and vapor–wall interaction and transport timescales nor for the significantly larger amount of absorbing mass of the chamber walls (relative to the deposited particles) for suspended vapors (McVay et al., 2014, 2016; Zhang et al., 2014).

In this study, we calculate SOA mass yields using the lower bound of the total SOA mass concentration obtained from SMPS measurements, which has been described in detail previously (Loza et al., 2012), and will be reviewed briefly here. For each particle size bin i at each time increment Δt, the particle number distribution deposited on the wall ($n_{w,i,j}$) is

$$n_{w,i,j} = n_{s,i,j} \times (1 - \exp(-\beta_i \Delta t)), \quad (1)$$

where $n_{s,i,j}$ is the suspended particle number distribution in particle size bin i at time step j, Δt is the difference between time step j and time step $j+1$, and β_i is the size-dependent first-order exponential wall loss rate obtained from seed-only experiments. As we describe subsequently, β_i may be measured directly during seed-only experiments or may be corrected for the influence of coagulation using a particle dynamics model. The particle wall-loss-corrected number distribution ($n_{\text{total},i,j}$) is obtained from the sum of the particle number distribution of deposited particles ($n_{w,i,j}$) and suspended particles ($n_{s,i,j}$):

$$n_{\text{total},i,j} = n_{s,i,j} + n_{w,i,j}. \quad (2)$$

Assuming spherical particles, the particle wall-loss-corrected volume concentration ($V_{\text{total},j}$) is

$$V_{\text{total},j} = \sum_{i=1}^{m} \frac{n_{\text{total},i,j}}{D_{\text{p},i} \ln 10} \times (D_{\text{p},i+} - D_{\text{p},i-}) \times \frac{\pi}{6} D_{\text{p},i}^3, \quad (3)$$

where m is the number of particle size bins, $D_{\text{p},i+}$ and $D_{\text{p},i-}$ are the upper and lower limits for size bin i, respectively, and $D_{\text{p},i}$ is the median particle diameter for size bin i. The term $D_{\text{p},i} \ln 10$ is needed to convert from a lognormal distribution. Figures S1–S4 and Table S1 in the Supplement show results from the particle wall loss correction. To calculate the SOA mass concentration ($\Delta M_{o,j}$), the SOA density (ρ_{org}) is multiplied by the difference of the particle wall-loss-corrected volume concentration ($V_{\text{total},j}$) and the initial seed volume concentration (V_{seed}):

$$\Delta M_{o,j} = \rho_{\text{org}} \times (V_{\text{total},j} - V_{\text{seed}}). \quad (4)$$

The measured densities of the α-pinene SOA are 1.39 and 1.37 g cm^{-3} for the 100 and 500 ppb O_3 experiments, respectively, and are within the range (i.e., 1.19 to 1.52 g cm^{-3}) reported in previous α-pinene ozonolysis studies (Bahreini et al., 2005; Kostenidou et al., 2007; Song et al., 2007; Shilling et al., 2009).

3 Vapor–particle dynamics model

A coupled vapor–particle dynamics model is used to evaluate the influence of seed aerosol surface area and oxidation rate on SOA formation in the α-pinene ozonolysis chamber experiments. This model is similar to that used in McVay et al. (2014), and will be briefly described here. Parameters from the experimental data (temperature, pressure, initial α-pinene concentration) are used as model inputs. The initial size distribution is set to that measured by the SMPS, with the exception of the two nucleation experiments. Because nucleation is not explicitly simulated, an approximation is used in which the smallest diameter bin is initialized with the total number of particles measured at the end of the experiment (see Table S1). In each simulation, the decay of α-pinene, the consumption of O_3, the SOA mass concentration, and the SOA mass yield are calculated throughout the duration of the experiment. We assume a linear injection rate of O_3 based on the time required to inject the desired O_3 concentration. For example, O_3 is injected at a rate of 500/54.25 ppb min^{-1} for the first 54.25 min during the 500 ppb O_3 experiments. O_3 simultaneously decays by reaction with α-pinene at a rate constant of 9.4×10^{-17} cm^3 molec.$^{-1}$ s^{-1} (Saunders et al., 2003). Modeled O_3 and α-pinene concentrations are compared with observed concentrations in Fig. S5. The good fit

of modeled and observed O_3 and α-pinene concentrations indicates that our representation of O_3 is appropriate. The $O_3 + \alpha$-pinene reaction is assumed to occur in a well-mixed chamber and produces five classes of first-generation products, which are grouped according to mass saturation concentrations, similar to the volatility basis set (VBS; Donahue et al., 2006): $> 10^3$ (assumed to be completely volatile), 10^2, 10, 1 and 0.1 $\mu g\,m^{-3}$. Branching ratios between these products are optimized to fit the experimental data. These branching ratios cannot be compared directly to previously reported VBS parameters for α-pinene ozonolysis (e.g., Henry et al., 2012) since VBS parameters are typically mass-based, while the branching ratios in the model are mole-based. Furthermore, the branching ratios here account for the influence of vapor wall deposition, while typical VBS parameters do not. We assume that these five classes of products have molecular weights 168, 184, 192, 200 and 216 $g\,mol^{-1}$ based on the group contribution method (Donahue et al., 2011). The first-generation products are assumed not to undergo further reaction with O_3 upon formation.

The aerosol dynamics in the chamber obey the aerosol general dynamic equation (Seinfeld and Pandis, 2006):

$$\left(\frac{\partial n\left(D_\mathrm{p},t\right)}{\partial t}\right)=\left(\frac{\partial n\left(D_\mathrm{p},t\right)}{\partial t}\right)_\mathrm{coag}+\left(\frac{\partial n\left(D_\mathrm{p},t\right)}{\partial t}\right)_\mathrm{cond/evap}+\left(\frac{\partial n\left(D_\mathrm{p},t\right)}{\partial t}\right)_\mathrm{wall\ loss}. \quad (5)$$

Coagulation is not considered in the present model; we address the potential impact of coagulation later in the paper. The change in particle number distribution due to particle wall loss is

$$\left(\frac{\partial n\left(D_\mathrm{p},t\right)}{\partial t}\right)_\mathrm{wall\ loss}=-\beta_j\left(D_\mathrm{p}\right)n(D_\mathrm{p}t), \quad (6)$$

where, as noted in Sect. 2.2, $\beta_j(D_\mathrm{p})$ is the size-dependent first-order wall loss rate coefficient obtained from fitting seed-only experiments. The rate at which vapor condenses onto a spherical aerosol particle is:

$$J_i = 2\pi D_\mathrm{p} D_i (G_i - G_i^\mathrm{eq}) F_\mathrm{FS} \quad (7)$$

where G_i is the concentration of gas-phase species i, G_i^eq is the saturation concentration of gas-phase species i, D_i is the gas-phase molecular diffusivity (assumed to be $3 \times 10^{-6}\,m^2\,s^{-1}$; McVay et al., 2014), and F_FS is the Fuchs–Sutugin correction for non-continuum gas-phase diffusion:

$$F_\mathrm{FS} = \frac{0.75\alpha_\mathrm{p}(1+Kn)}{Kn^2 + Kn + 0.283Kn\alpha_\mathrm{p} + 0.75\alpha_\mathrm{p}} \quad (8)$$

where α_p is the vapor–particle mass accommodation coefficient and Kn is the Knudsen number, $Kn = 2\lambda_\mathrm{AB}/D_\mathrm{p}$. The vapor–particle mass accommodation coefficient accounts for any resistance to vapor molecule uptake at the particle surface (e.g., surface accommodation and particle-phase diffusion limitations). λ_AB is the mean free path of the gas-phase species, which is

$$\lambda_\mathrm{AB} = 3D_i \times \sqrt{\frac{\pi M_i}{8RT}}, \quad (9)$$

where R is the ideal gas constant, T is the temperature, and M_i is the molecular weight of diffusing gas-phase molecule i. For each particle size bin, Eqs. (7)–(9) are used to compute the flux of each gas-phase species to and from an aerosol particle, scaled by the particle number concentration in the size bin. The net rate of change for each gas-phase species due to evaporation or condensation is obtained from the total flux summed over all the particle size bins.

G_i^eq varies for each particle size bin because it depends on the mass concentration of species i and the total organic mass concentration in the size bin:

$$G_i^\mathrm{eq} = \frac{A_i C_i^*}{\sum_k A_k + M_\mathrm{init}}, \quad (10)$$

where A_i is the concentration of species i in the particle phase, C_i^* is the saturation concentration of species i, $\sum_k A_k$ is the sum of all the species concentration in the particle phase, and M_init is the mass concentration of any absorbing organic material initially present in the seed aerosol. To avoid numerical errors in Eq. (10) at the first time step, M_init is set to 0.01 $\mu g\,m^{-3}$.

The oxidation products of α-pinene ozonolysis are assumed to be subject to vapor wall deposition, which is simulated using a first-order wall loss coefficient (McMurry and Grosjean, 1985):

$$k_\mathrm{wall,on} = \left(\frac{A}{V}\right)\frac{\frac{\alpha_\mathrm{wall}\bar{c}}{4}}{1+\frac{\pi}{2}\left(\frac{\alpha_\mathrm{wall}\bar{c}}{4\sqrt{k_\mathrm{e}D_i}}\right)}, \quad (11)$$

where A/V is the surface area-to-volume ratio of the chamber (estimated to be $2.5\,m^{-1}$), α_wall is the vapor–wall mass accommodation coefficient, and k_e is the eddy diffusion coefficient that describes mixing conditions in the chamber. Based on the measured size-dependent particle wall loss rates (method is described in Zhang et al., 2014), k_e is estimated to be $0.03\,s^{-1}$ for the GTEC chamber. Vapor wall deposition is assumed to be reversible, and the rate constant of vapor desorption from the chamber walls is

$$k_\mathrm{wall,off} = \frac{k_\mathrm{wall,on}}{K_\mathrm{w}C_\mathrm{w}} = k_\mathrm{wall,on}\left(\frac{C_i^* M_\mathrm{w}\gamma_\mathrm{w}}{C_\mathrm{w}M_\mathrm{p}\gamma_\mathrm{p}}\right), \quad (12)$$

where C_w is the equivalent organic mass concentration in the wall (designated to treat gas–wall partitioning in terms of gas–particle partitioning theory and not necessarily representative of a physical layer of organic concentration on the wall;

Matsunaga and Ziemann, 2010), K_w is the gas–wall partitioning coefficient, M_w is the effective molecular weight of the wall material, γ_w is the activity coefficient of the species in the wall layer, M_p is the average molecular weight of organic species in the particle, and γ_p is the activity coefficient of the species in the particle. For simplicity, we assume that $M_w = M_p$ and $\gamma_w = \gamma_p$. C_w is set to 10 mg m^{-3} based on previous inferences by Matsunaga and Ziemann (2010). Sensitivity studies (not shown) show no change in model predictions when varying C_w above $C_w = 0.1$ mg m^{-3}.

In the initial version of the model, after all the α-pinene is consumed, vapor wall deposition was assumed to continue to deplete the gas-phase oxidation products and aerosol mass evaporates to maintain gas–particle equilibrium. SOA evaporation was not observed experimentally (i.e., the SOA mass concentration does not decrease significantly over time after peak SOA growth has been achieved in these chamber experiments; Fig. 2). In order to represent these observations in the model, a first-order, particle-phase reaction is introduced by which aerosol species are converted into non-volatile absorbing organic mass with a timescale of τ_{olig}. This mechanism (which is not included in the model used in McVay et al., 2014) is similar to that used by the sequential equilibrium partitioning model, in which aerosol is converted from an absorbing to non-absorbing, non-volatile phase in order to explain the inhibited diffusion and evaporation observed in α-pinene ozonolysis SOA (Cappa and Wilson, 2011). Although we assume here that the converted non-volatile aerosol mass still participates in partitioning, either mechanism invokes a particle-phase process to retard SOA evaporation.

In order to determine the parameters for α_w, α_p, τ_{olig} and the branching ratios between the oxidation products that provide the best fit to measured SOA data, the parameter space was discretized and all possible combinations of parameters were simulated, following Karnezi et al. (2014). In order to restrict the number of combinations required, only parameter values judged to be physically realistic were chosen. Because the branching ratios in this model are mole-based, they must sum to one; therefore only combinations of parameters summing to one were allowed. The discretization is shown in Table S2 and results in roughly 10 000 different combinations of parameters. All six experiments were simulated with each parameter combination, and simulations were run using GNU parallel (Tange, 2011). For each combination of parameters, the percentage error was calculated from Eq. (10) of Karnezi et al. (2014):

$$E_i = \frac{100}{n}\sqrt{\sum_{i}^{n}(\mathrm{Moa}_{i,\mathrm{guess}} - \mathrm{Moa}_{i,\mathrm{meas}})^2}, \quad (13)$$

where $\mathrm{Moa}_{i,\mathrm{guess}}$ is the model-predicted SOA mass concentration at a particular time step i for one of the experiments, $\mathrm{Moa}_{i,\mathrm{meas}}$ is the measured SOA mass concentration at a particular time step i for one of the experiments, and n is the number of time steps summed over all experiments. The best-fit combination of parameters is defined as the combination of parameters with the lowest percentage error. This lowest-error combination of parameters was compared to the "best-estimate" parameters determined from the inverse error weighting factor of Karnezi et al. (2014):

$$\bar{x} = \frac{\sum_{j}^{N}\left[x_j \frac{1}{E_j}\right]}{\sum_{j}^{N}\frac{1}{E_j}}, \quad (14)$$

where x_j is a value of one of the parameters (α_w, α_p, τ_{olig} or a branching ratio between the oxidation products), with N different possible combinations of parameters, and E_j is the percent error for that particular combination of parameters. The lowest-error combination of parameters and the Karnezi et al. (2014) best-estimate parameters are both reported, but the lowest-error combination of parameters resulted in a lower percentage error than the Karnezi et al. (2014) best-estimate parameters. The lowest-error combination of parameters is used for the modeling analysis (Table 2).

4 Results

Red and blue solid lines in Fig. 1 shows the size-dependent particle wall deposition coefficients measured in the low AS-seed-only and high AS-seed-only deposition experiments. In these measurements, we assume that the number concentration is low enough such that the effect of coagulation is small and only particle wall deposition affects the particle size distribution, thus allowing for the direct measurement of size-dependent particle wall deposition coefficients. The initial total AS seed surface area concentration in the low AS-seed-only and high AS-seed-only experiments (which are conducted using 0.015 and 0.05 M AS solutions, respectively) are similar to those used in the α-pinene ozonolysis experiments (i.e., $\sim$ 1000 and $\sim$ 3000 µm^2 cm^{-3}, respectively). As shown in Fig. 1, the measured particle wall deposition coefficients from the low AS-seed-only and high AS-seed-only experiments generally fall within the range of those measured in routine monthly AS-seed-only experiments conducted in the chamber. Figure 1 also shows the size-dependent particle wall deposition coefficients corrected for coagulation, shown using dashed lines, which are obtained as described in Pierce et al. (2008) using the data from the low AS-seed-only and high AS-seed-only experiments. A comprehensive description of the relationship between coagulation and particle wall deposition will be provided in a forthcoming publication. Briefly, as described in Pierce et al. (2008), the coagulation-corrected particle wall loss coefficients are determined by simulating the decay of the initial size distribution due to coagulation and then attributing the difference in this decay and the observed decay to particle wall loss. For both the measured and coagulation-corrected particle wall deposition

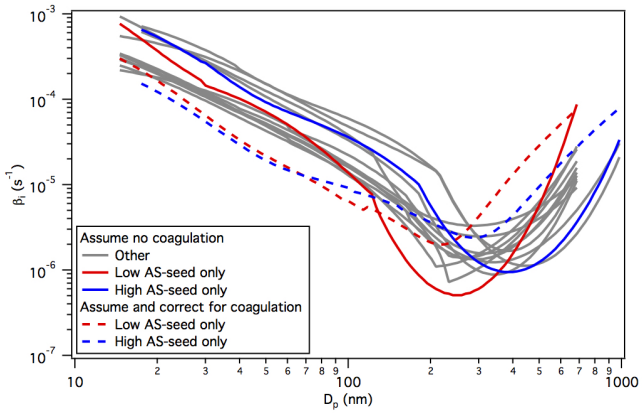

Figure 1. Particle wall deposition coefficients (β_i) measured during the low AS-seed-only and high AS-seed-only experiments in GTEC. Also shown are the particle wall deposition coefficients (labeled "Other") measured in previous routine monthly AS-seed-only experiments in the chamber. These previous routine monthly AS-seed-only experiments were performed using either a 0.008 M AS or a 0.1 M AS solution. Coagulation-corrected particle wall deposition coefficients (see Pierce et al., 2008, and main text for details) are also shown, using dashed lines.

coefficients, the minimum coefficient for the low AS-seed-only experiment is different from that of the high AS-seed-only experiments. The cause of this difference is currently under investigation but may be due in part to uncertainties arising from the low particle number concentrations for the larger particles in the low AS-seed-only experiment. To study how coagulation can potentially affect SOA mass yields in this study, both the measured and coagulation-corrected size-dependent particle wall deposition coefficients are used to correct for particle wall deposition in the α-pinene ozonolysis experiments.

Assuming that the effect of coagulation is small, the particle wall-deposition-corrected number concentration data provide a test of the appropriateness of the particle wall deposition correction. The corrected number concentration should level off at a constant value (i.e., the initial particle number concentration), assuming no significant coagulation, when particle wall deposition is properly accounted for since the wall-deposited particle number distribution is added to the suspended particle number distribution during particle wall loss correction. Neglecting coagulation, we account for particle wall deposition in nucleation and low-AS experiments using deposition coefficients measured from the low AS-seed-only experiments, while particle deposition in high-AS experiments are accounted for using coefficients measured from the high AS-seed-only experiments. Figures S1 and S2 show the particle wall deposition-corrected aerosol number and volume concentrations. Over all experiments, the particle wall deposition-corrected final particle number concentration (i.e., at the end of the reaction) is 9 to 17 % less than the initial particle number concentration for the low-AS and high-AS experiments (Table S1), respectively, indicating that the particle wall deposition-corrected volume concentrations are slightly underestimated. The fact that the particle wall deposition-corrected final particle number concentrations are somewhat smaller than the initial particle number concentrations may be due to variations in particle wall deposition rates in the AS-seed-only and α-pinene ozonolysis experiments or to coagulation. To first examine variations in particle wall deposition rates, we used the average of the measured low AS-seed-only and high AS-seed-only particle wall deposition coefficients to account for particle wall deposition in all the experiments (Figs. S3 and S4). While there is a negligible difference in the particle wall-deposition-corrected volume concentrations (Figs. S3 and S4 vs. Figs. S1 and S2), a larger spread (1 to 22 %) exists in the difference between the initial and final particle number concentrations when the average measured particle wall deposition coefficients are used (Table S1). Therefore, all subsequent nucleation and low-AS data presented here are particle wall deposition-corrected using coefficients measured from the low AS-seed-only experiments, and all high-AS data are corrected using particle wall deposition coefficients measured from the high AS-seed-only experiments. We furthermore conclude that variations in particle wall deposition rates do not cause the decrease in the particle wall deposition-corrected final number concentration, which is most likely due to coagulation. Thus, the SOA data are also corrected using the coagulation-corrected particle wall deposition coefficients (discussed below). We show subsequently the relatively minor difference that correcting for coagulation has on overall SOA mass yields. Therefore, we use SOA concentrations corrected using the measured particle wall deposition coefficients for the bulk of the analysis in this study.

Figure 2 shows the reaction profiles of the α-pinene ozonolysis experiments. SOA growth typically starts within 10 to 20 min of the start of the reaction. At either O_3 concentration, the molar ratio of O_3 reacted to α-pinene reacted is approximately 1 : 1 (i.e., 50 ppb α-pinene reacted with 50 ppb O_3), which indicates that O_3 reacts only with α-pinene and not its oxidation products. As anticipated, the α-pinene oxidation rates in the 100 ppb O_3 experiments are significantly slower than those in the 500 ppb O_3 experiments. Figure 2a–c show that peak SOA levels are typically reached at reaction time $\sim$ 300 to 350 min in the 100 ppb O_3 experiments, during which $\geq$ 95 % of the injected α-pinene has reacted. In contrast, all the α-pinene reacts within 80 to 90 min of the start of reaction in the 500 ppb O_3 experiments, and peak SOA levels are achieved at reaction time $\sim$ 100 min (Fig. 2d–f). These results indicate that the O_3 concentration dictates both the rate of α-pinene oxidation and the time it takes to achieve peak SOA growth.

Figure 3 shows the time-dependent growth curves (SOA mass concentration vs. α-pinene reacted; Ng et al., 2006) for the 100 and 500 ppb O_3 experiments. Only SOA growth data

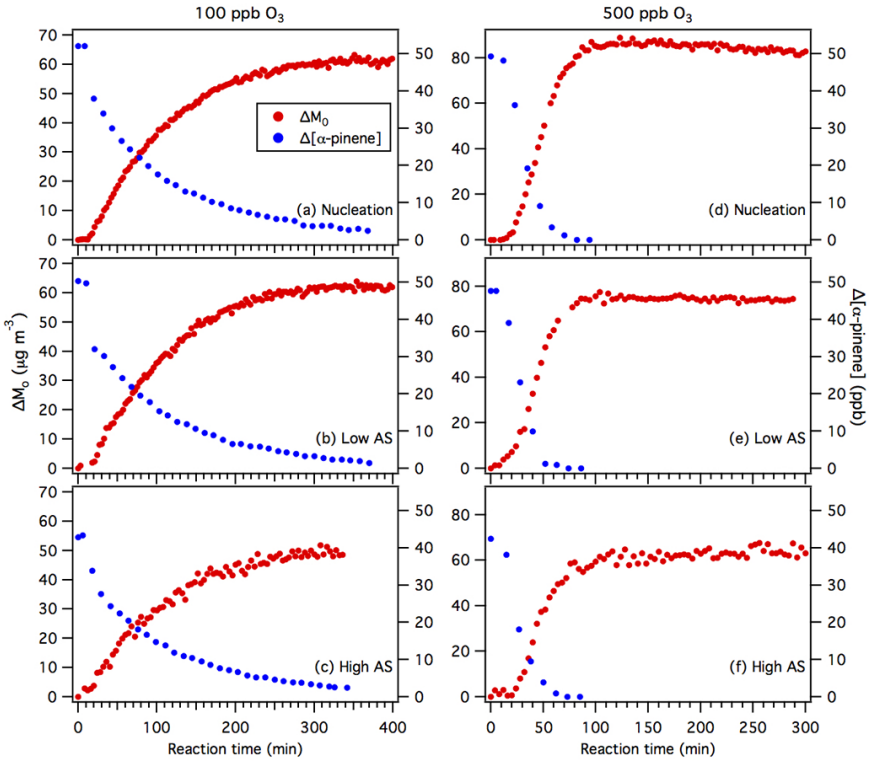

Figure 2. Reaction profiles of the α-pinene ozonolysis experiments. Panels **(a, b, c)** show results from the nucleation, low-AS and high-AS 100 ppb O_3 experiments, respectively. Panels **(d, e, f)** show results from the nucleation, low-AS and high-AS 500 ppb O_3 experiments, respectively. As explained in the main text, the SOA mass concentrations (ΔM_o) for the nucleation and low-AS experiments are obtained using the particle wall deposition rates obtained from the low AS-seed-only experiments, while the SOA mass concentrations (ΔM_o) for the high-AS-seed experiments are obtained using the particle wall deposition rates obtained from the high AS-seed-only experiments.

up to SOA peak concentrations are shown. SOA growth essentially stops once all the α-pinene has reacted. This is expected, as α-pinene has only one double bond; the first step of α-pinene ozonolysis is rate-limiting and the first-generation products are condensable (Ng et al., 2006; Chan et al., 2007). The time-dependent SOA growth curves for experiments corresponding to different seed aerosol concentrations overlap for both low and high O_3 concentrations. This indicates that the initial AS seed surface area does not influence the SOA growth rate within the range of AS seed surface area concentration used. It is important to note that while it appears that the SOA growth rate is faster in the 100 ppb O_3 relative to the 500 ppb O_3 experiments based on the time-dependent growth curves shown in Fig. 3, this is not the case. Instead, the observed time-dependent growth curves can be explained by the higher concentration of α-pinene having reacted during the 10 to 20 min delay of SOA formation in the 500 ppb O_3 experiments compared to the 100 ppb O_3 experiments (Fig. 2).

Figure 4 shows the time-dependent SOA mass yields as a function of initial total AS seed surface area for the 100 and 500 ppb O_3 experiments. Regardless of the O_3 concentration, the SOA mass yields stay roughly constant despite the increase in AS seed surface area. This indicates that the surface area concentration of AS seed aerosol does not noticeably influence the partitioning of gas-phase α-pinene ozonolysis products to the particle phase within the range of AS seed surface area concentration used. Higher SOA mass yields are observed in the 500 ppb O_3 experiments, which indicates that the α-pinene oxidation rate controls the absolute amount of SOA formed. It is important to note that these conclusions are robust even when the average of the measured low AS-seed-only and high AS-seed-only particle wall loss coefficients is used to account for particle wall loss in all the experiments (Fig. S6). The enhancement of SOA mass yields at higher O_3 concentrations and the lack of a SOA mass yield dependence on AS seed surface area (within the range of AS seed surface area concentration used in this study) will be discussed further in Sect. 5.

The α-pinene ozonolysis SOA mass yields obtained in this study are compared to those reported in previous studies in Fig. 5. Table S3 lists the experimental conditions employed in these studies. To facilitate comparison between the different studies, all the SOA mass yield and concentration data (including this study) are adjusted to an organic density of 1.0 g cm^{-3}. As shown in Fig. 5, the SOA mass yields obtained at peak SOA growth in this study are generally con-

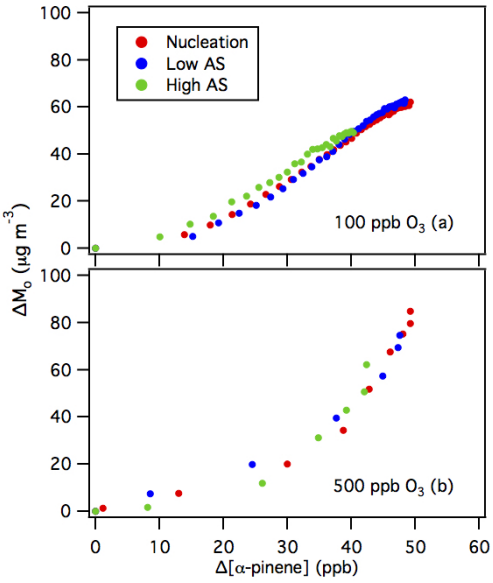

Figure 3. Time-dependent SOA growth curves for α-pinene ozonolysis. Panels **(a, b)** show 10 min averaged results from the 100 and 500 ppb O_3 experiments, respectively. Only SOA growth data up to the point of SOA peak growth are shown.

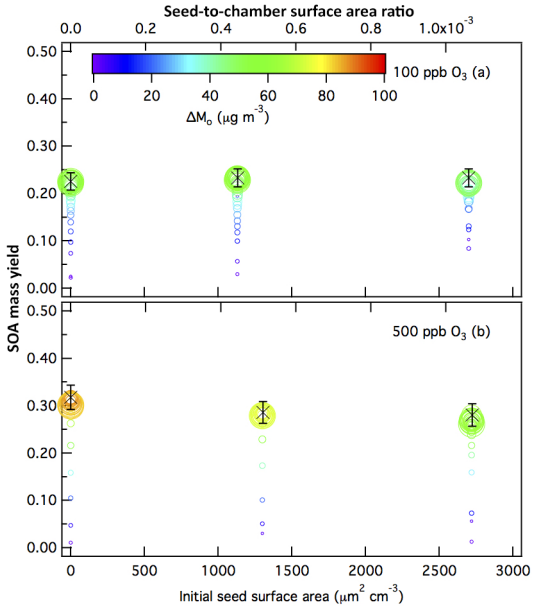

Figure 4. Ten-minute-averaged SOA mass yields over the course of an α-pinene ozonolysis experiment as a function of initial total AS seed surface area concentration for the **(a)** 100 ppb O_3 experiments, and **(b)** 500 ppb O_3 experiments. Symbol color indicates the SOA mass concentration and symbol size indicates the time after O_3 is injected into the chamber. The $\times$ symbols are the SOA mass yields at peak SOA growth obtained from the experimental data. The y-axis error bars represent the uncertainty in the SOA mass yield at peak SOA growth, which originates from the α-pinene injection and the aerosol volume concentration measured by the SMPS at peak SOA growth (1 standard deviation).

sistent with those of previous studies where the chamber was operated in batch mode (that in this study).

To investigate the influence of coagulation on the SOA mass yields, the coagulation-corrected size-dependent particle wall deposition coefficients are also used to correct for particle wall deposition in the α-pinene ozonolysis experiments. Specifically, all nucleation and low-AS data are particle wall deposition-corrected using coagulation-corrected coefficients derived from the low AS-seed-only experiments, and all high-AS data are corrected using coagulation-corrected particle wall deposition coefficients derived from the high AS-seed-only experiments. Figure S7 shows the time-dependent SOA mass yields (obtained using the coagulation-corrected and measured particle wall deposition coefficients) as a function of initial total AS seed surface area. SOA mass yields obtained using the coagulation-corrected particle wall deposition coefficients are < 2 % (absolute values) higher than those using the measured particle wall deposition coefficients. Similar to the SOA mass yields obtained using the measured particle wall deposition coefficients (Figs. 4, S7c and d), SOA mass yields obtained using the coagulation-corrected particle wall deposition coefficients stay roughly constant despite the increase in AS seed surface area for both O_3 concentrations, and the SOA mass yields are higher in the 500 ppb O_3 experiments (Fig. S7a and b). The mass yields obtained at peak SOA growth are also generally consistent with those of previous studies (Fig. S8). Taken together, this suggests that the effect of coagulation on the SOA mass yields is likely minor for the aerosol concentrations used in this study. Therefore, only data that have been particle wall deposition-corrected using coefficients measured in the low AS-seed-only and high AS-seed-only experiments are fitted to determine model parameters for the vapor–particle dynamics model described in Sect. 3.

As noted earlier, optimal model values for α_p, α_w, τ_{olig} and the branching ratios between the oxidation products were determined by calculating the error between the observed and modeled time-dependent SOA concentrations for all possible combinations of model parameters. The combination of parameters with the lowest percent error is $\alpha_w = 10^{-6}$, $\alpha_p = 0.1$, $\tau_{olig} = 4$ h, with branching ratios = 0.6, 0.3, 0.05, 0.05 and 0 for oxidation products with vapor pressures $> 10^3$, 10^2, 10, 1 and 0.1 μg m^{-3}, respectively. This combination of parameters results in a percent error of 21 % (Table S4). It is important to note that predictions using $\alpha_p = 0.1$ or 1 resulted in very similar errors; with the same combination of parameters and $\alpha_p = 1$, the percent error only increased to 22 %. The best-estimate parameters determined following the Karnezi et al. (2014) method are as follows: $\alpha_w = 3.6 \times 10^{-6}$, $\alpha_p = 0.35$, $\tau_{olig} = 6$ h, with branching ratios = 0.66, 0.16, 0.06, 0.06, and 0.06 for oxidation products with vapor pressures $> 10^3$, 10^2, 10, 1 and 0.1 μg m^{-3}, respectively. This combination of parameters results in an error

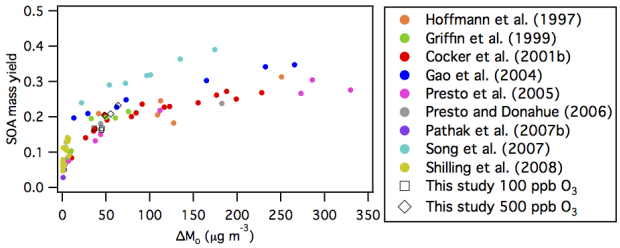

Figure 5. Comparison of SOA mass yields obtained in this study to those of previous dark α-pinene ozonolysis studies (Table S3). The SOA mass yields and concentrations of majority of these previous studies (Hoffmann et al., 1997; Griffin et al., 1999; Cocker et al., 2001b; Gao et al., 2004; Presto et al., 2005; Presto and Donahue, 2006; Pathak et al., 2007b; Song et al., 2007) were previously compiled by Shilling et al. (2008). Similar to Shilling et al. (2008), all the data shown here (including those reported in this study) have been adjusted using an organic density of 1.0 g cm^{-3}, and to 298 K using a temperature correction of 1.6 % K^{-1}, as recommended by Pathak et al. (2007b) to facilitate easier comparison among the different studies.

of 37 % (Table S4). Model predictions using both sets of parameters are compared to measured SOA concentrations in Fig. S9. The lowest-error parameters are used for the analysis in the remainder of this study (Table 2). The best-fit $\alpha_w = 10^{-6}$ corresponds to a first-order vapor wall deposition rate constant ($k_{wall,on}$) of 10^{-4} s^{-1}. A wide range of vapor wall loss rates has been reported (Fig. 3 of Krechmer et al., 2016). This $k_{wall,on}$ value is comparable to that reported by Matsunaga and Ziemann (2010) for an 8.2 m^3 chamber but significantly faster than wall loss rates that have been measured in the Caltech chamber (Zhang et al., 2015a). The reason for this wide range of reported vapor wall loss rates is currently uncertain and outside the scope of this study.

5 Discussion

α-pinene ozonolysis has been carried out at two O_3 mixing ratios (100 and 500 ppb) under varying AS seed aerosol surface area concentrations (0, ~1000 and ~3000 μm^2 cm^{-3}).

5.1 Seed aerosol surface area effect

Figure 3 shows that the time-dependent SOA growth curves for experiments with different seed area concentrations overlap at both O_3 concentrations, which indicates the AS seed surface area does not affect the rate of SOA growth within the range of AS seed surface area concentration used in this study. This observation differs from findings by Pathak et al. (2007b) for the $O_3 + \alpha$-pinene system, who showed that even though the final SOA mass yields measured in the reaction of 7.3 ppb α-pinene with 1500 ppb O_3 were similar in their seeded and unseeded experiments, SOA growth was considerably slower in unseeded experiments compared to seeded experiments. The authors suggested that the slow SOA formation rate in their unseeded experiment was the result of SOA formation being limited by the mass transfer of semi-volatile oxidation products to newly formed particles (via nucleation) during the early stages of the experiment. These newly formed particles have a significantly smaller aerosol surface area for gas–particle partitioning as compared to that of seed aerosol particles in the seeded experiments. Consequently, the semi-volatile oxidation products accumulated in the gas phase during the early stages of the unseeded experiments, resulting in slower SOA growth compared to the seeded experiments. The observation that the presence of seed aerosol does not influence the SOA growth rate in the present study may be explained by the relatively high concentrations of α-pinene reacted and SOA mass loadings obtained. Previous studies have shown that the delay between the onset of VOC oxidation and SOA formation in unseeded experiments is most pronounced at low aerosol loadings (Kroll et al., 2007). We note that the concentrations of α-pinene reacted and SOA mass loadings obtained in this study are significantly larger than those reported by Pathak et al. (2007b). Therefore, it is possible that, due to the relatively large concentrations of α-pinene reacted in this study, substantial concentrations of gas-phase oxidation products are generated, which results in rapid partitioning into the particle phase even in the absence of seed aerosol. This is evident from the large increase in the particle number concentration during the early stages of the unseeded 100 and 500 ppb O_3 experiments, where the particle number concentration increased to ~8000 and ~10 000 particles cm^{-3} during the first 45 min of the 100 and 500 ppb O_3 experiments, respectively (Figs. S1a and S2a). Thus, the SOA growth rates are not controlled by the presence of AS seed in this study.

Figure 4 shows that, for both O_3 mixing ratios used, the time-dependent SOA mass yield is similar at any given AS seed surface area (see also Table 1). The absence of a SOA growth dependence on the AS seed surface area is similar to observations reported by McVay et al. (2016) for the α-pinene photooxidation (OH-driven chemistry) system but differs from those reported by Zhang et al. (2014) for the toluene photooxidation system in which the SOA mass yield increased with the surface area concentration of seed aerosol.

The best-fit $\alpha_p = 0.1$ (or $\alpha_p = 1$, with almost the same percentage error) suggests the absence of significant limitations to vapor-particle mass transfer in the present α-pinene ozonolysis study, and that SOA formation is governed by quasi-equilibrium growth (Saleh et al., 2013; McVay et al., 2014), which occurs when SOA-forming vapors are produced at a rate that is significantly slower than that required to establish gas–particle equilibrium (Shiraiwa and Seinfeld, 2012; Zhang et al., 2012). Moreover, the characteristic timescale to establish gas–particle equilibrium is less than those for reaction and vapor wall deposition. When the vapor and particle phases maintain equilibrium, gas–particle equilibrium is controlled by the amount of organic matter

in the VOC system. As a result, the rate of condensation of SOA-forming vapors is independent of the seed aerosol surface area (McVay et al., 2014). The best-fit $\alpha_p = 0.1$ is within the range of α_p coefficients determined from α-pinene ozonolysis SOA thermodenuder studies ($\alpha_p = 0.1$) (Saleh et al., 2013; Saha and Grieshop, 2016) and α-pinene photooxidation chamber studies ($\alpha_p = 0.1$ or 1) (McVay et al., 2016). Notably, this result differs markedly from that for toluene photooxidation (Zhang et al., 2014), where α_p was determined to be 0.001, and for which, since the SOA mass yield was strongly dependent on the seed aerosol surface area, the condensation of SOA-forming vapors onto seed aerosol particles was kinetically limited (McVay et al., 2014). Kinetically limited SOA growth occurs when the timescale for gas–particle equilibrium is competitive with or exceeds the timescale for reaction and vapor wall deposition and may reflect imperfect accommodation of gas-phase organics to the particle phase. The markedly different behavior of the α-pinene and toluene SOA systems could be due to differences in SOA volatility and aerosol physical phase state (McVay et al., 2016).

5.2 Oxidation rate effect

At higher O_3 concentrations, the α-pinene oxidation rate increases, leading to higher SOA mass yields (the "oxidation rate" effect). This behavior was previously observed by Ng et al. (2007) for the *m*-xylene photooxidation system, for which the oxidation rate effect was attributed to the loss of semivolatile condensable products to chamber walls in competition with condensation onto seed particles to form SOA.

SOA formation from α-pinene ozonolysis is presumed to be driven by a range of semi- and low-volatility first-generation products arising from reaction of O_3 with the single C=C double bond (Ng et al., 2006). These products are subject to two competing routes: condensation to particles to form SOA or deposition on the chamber walls. Each process can be represented in terms of a first-order rate constant: $k_{wall,on}$ and $k_{particle,on}$ (s^{-1}). The rate of vapor wall deposition of condensable species A is then $k_{wall,on} \times [A]$ (molec cm^{-3} s^{-1}) and the rate of condensation onto particles is $k_{particle,on} \times [A]$ (molec cm^{-3} s^{-1}). Increasing the rate of reaction increases the concentration of $[A]$, but the relative rates of vapor wall deposition and condensation onto particles will remain the same. In general, however, both vapor wall deposition and vapor particle condensation are reversible processes (McVay et al., 2014; Zhang et al., 2014). The first-order rate constant for evaporation from the wall can be represented as (Matsunaga and Ziemann, 2010)

$$k_{wall,off} = k_{wall,on}\left(\frac{C_i^*}{C_w}\right), \quad (15)$$

where C_i^* is the saturation concentration and C_w is the assumed equivalent wall organic concentration. The rate of evaporation from particles is

$$k_{particle,off} = k_{particle,on}\left(\frac{C_i^*}{C_{aer}}\right), \quad (16)$$

where C_{aer} is the organic aerosol concentration ($C_{aer} = \sum A_k + M_{init}$).

The difference between C_{aer} and C_w is the key to explaining the oxidation rate effect. At the beginning of the experiment, C_{aer} is very small because the inorganic seeds are essentially non-absorbing. Therefore, $k_{particle,off}$ is large, and the net SOA growth is small. In contrast, C_w is considered to be substantial (on the order of 10 mg m^{-3}) and to be essentially constant throughout the experiment (Matsunaga and Ziemann, 2010; McVay et al., 2014; Zhang et al., 2014). Model predictions are insensitive to the value of C_w since, in any event, C_w is significantly larger than C_{aer} (Zhang et al., 2014). Therefore, $k_{wall,off}$ is small at the beginning of the experiment and the net vapor wall loss rate is fast. As C_{aer} increases, the net SOA condensation rate increases relative to the net vapor wall loss rate. When the reaction rate increases corresponding to higher O_3 concentrations, C_{aer} grows more quickly because more condensable species are available to form SOA, and the net condensation rate increases more rapidly. Therefore, the observed oxidation rate effect is due to vapor wall deposition, and arises because vapor–particle partitioning and vapor wall condensation are essentially reversible processes. This explanation is consistent with simulations varying the O_3 concentration in which all species are non-volatile (i.e., do not evaporate from the particles or the wall). In this case, no oxidation rate effect is observed as the O_3 concentration increases. The growth curves for different O_3 concentrations overlap, and the same yield is obtained regardless of O_3 concentration (Fig. S10).

Sensitivity tests were performed to determine the point at which SOA formation is no longer influenced by the O_3 concentration. In these simulations, the initial α-pinene concentration is fixed at 48 ppb, while the O_3 concentration is varied from 75 to 1000 ppb. The rate of O_3 injection is assumed to remain constant as the O_3 concentration is increased to mimic the experimental protocol (i.e., O_3 injection time is increased to achieve higher O_3 concentrations). The O_3 injection rate used in these simulations is fixed at 500/54.25 ppb min^{-1}, which is the same as that used to analyze results from the 500 ppb O_3 experiments. Model predictions in Fig. S11 show that the maximum SOA mass concentration increases with increasing O_3 concentration up to approximately 500 ppb O_3. Beyond this O_3 concentration, the SOA growth curves overlap and the maximum SOA mass concentration does not increase even when more O_3 is added. This plateau arises due to the lengthening time required to inject increasing amounts of O_3. More than 1 h is required to inject > 500 ppb of O_3, and by this time virtually all of the α-pinene has reacted. Increasing the O_3 concentration after all of the α-pinene has reacted does not lead to any changes in the SOA mass concentration. However, if a faster injec-

tion rate of O_3 is used, the oxidation rate effect will persist to higher O_3 concentrations (i.e., > 500 ppb O_3) (Fig. S12). With a faster injection rate, 500 ppb O_3 is injected before all of the α-pinene has reacted. Continuing to inject O_3 to a higher concentration (i.e., 750 ppb) will cause α-pinene to decay faster and SOA to grow faster than when the O_3 injection stops at 500 ppb. The oxidation rate effect is then apparent at higher O_3 concentrations. If, instead of using an injection rate of O_3, simulations are run using fixed initial O_3 (not possible experimentally), the rate effect persists to even higher O_3 concentrations. The relative increase in yield with increasing O_3 concentrations slows at very high O_3 concentrations because the rate of reaction becomes substantially faster than the vapor wall deposition rate, and there is less marginal effect to increasing the reaction rate.

It should be noted that while we showed that the observed oxidation rate effect (i.e., higher SOA mass yields as a result of faster hydrocarbon oxidation rates) is a consequence of vapor wall deposition, the possibility that differing peroxy radical (RO_2) chemistry in the 100 and 500 ppb O_3 experiments may play some role in influencing the SOA mass yields cannot be discounted. RO_2 radicals, which are formed from the decomposition of excited Criegee intermediates (Docherty et al., 2005), may be produced at faster rates in the 500 ppb O_3 experiments. This may lead to the higher production of condensable oxidation products from the $RO_2 + RO_2$ reaction pathway in the 500 ppb O_3 experiments (relative to those formed in the 100 ppb O_3 experiments), which may result in higher SOA mass yields.

5.3 Interplay of the seed aerosol surface area effect and the oxidation rate effect

In this study, we observe an oxidation rate effect but not a seed aerosol surface area effect. In Zhang et al. (2014), a seed aerosol surface area effect was observed, but the variation of the oxidation rate was not studied. A key aspect of vapor wall deposition is the potential interplay between the seed aerosol surface area effect and the oxidation rate effect. To examine this interplay in the α-pinene ozonolysis system, simulations were carried out by varying the seed aerosol surface area and the O_3 concentration simultaneously, while using the branching ratios, oligomerization rate, and vapor wall deposition rate parameters obtained in the present study. The initial α-pinene concentration was set to 50 ppb, and a fixed O_3 concentration was used in place of a linear injection. α_p was varied at 0.001, 0.01, 0.1, and 1 in these simulations. Figure 6 shows the SOA mass yield at peak SOA growth as a function of both the seed aerosol surface area and O_3 concentration for $\alpha_p = 1$, 0.1, 0.01, and 0.001. For $\alpha_p = 1$ or 0.1, the oxidation rate dominates: SOA mass yield increases significantly as O_3 concentration increases, while the seed aerosol surface area has a negligible effect. For $\alpha_p = 0.01$, both effects can be observed in different regions: at low O_3 concentrations and high seed aerosol surface areas, the oxidation rate effect dominates; at low seed aerosol surface areas and high O_3 concentrations, the seed surface area dominates. At low seed aerosol surface areas and low O_3 concentrations, both effects are present. For $\alpha_p = 0.001$, the seed aerosol surface area effect dominates except at very high seed aerosol surface areas. These observations show that the presence of an oxidation rate effect and/or seed aerosol surface area effect depends on a complex interplay of factors, such as α_p, the rate of hydrocarbon oxidation, and the amount of seed surface area present.

6 Implications

In this study, we systematically examine the roles of gas–particle partitioning and VOC oxidation rate in the presence of vapor wall deposition in α-pinene ozonolysis. We show that despite the presence of vapor wall deposition, SOA mass yields at peak SOA growth remain approximately constant regardless of the seed aerosol surface area (within the range of AS seed surface area concentration used in this study). This observation is consistent with SOA formation in the α-pinene ozonolysis system being governed by quasi-equilibrium growth, for which there are no substantial limitations to vapor-particle mass transfer. This result was demonstrated in a previous modeling study which showed that increasing the seed-to-chamber surface area ratio will lead to increased SOA growth only in cases in which the condensation of SOA-forming vapors onto seed aerosol particles is kinetically limited as a result of imperfect accommodation of gas-phase organics to the particle phase (McVay et al., 2014).

An important implication of this study is that diverting vapor wall deposition in chamber studies via the addition of ever-increasing quantities of seed aerosol particles is not effective in VOC systems for which SOA formation is governed by quasi-equilibrium growth. This study also underscores the importance of accounting for particle wall deposition appropriately in chamber studies in order to avoid erroneous conclusions regarding the role of gas–particle partitioning (quasi-equilibrium vs. kinetically limited SOA growth) in influencing vapor wall loss in the VOC system.

We note that the present study shows that the SOA mass yield is independent of seed aerosol surface area concentration for values ranging from 0 to $\sim 3000\,\mu m^2\,cm^{-3}$. This corresponds to a seed-to-chamber surface area ratio of 0 to $\sim 1 \times 10^{-3}$, which is substantially smaller than the range used by Zhang et al. (2014) to study the influence of vapor wall deposition on toluene photooxidation SOA formation in the Caltech chamber (i.e., 0 to $\sim 5 \times 10^{-3}$). It is possible that a SOA mass yield dependence on the seed surface area may have become more apparent had a larger range of seed aerosol surface area (i.e., $> 3000\,\mu m^2\,cm^{-3}$), and hence a larger range of seed-to-chamber surface area ratio, been used here. One consideration is that coagulation may become increasingly important, and will need to be accounted for,

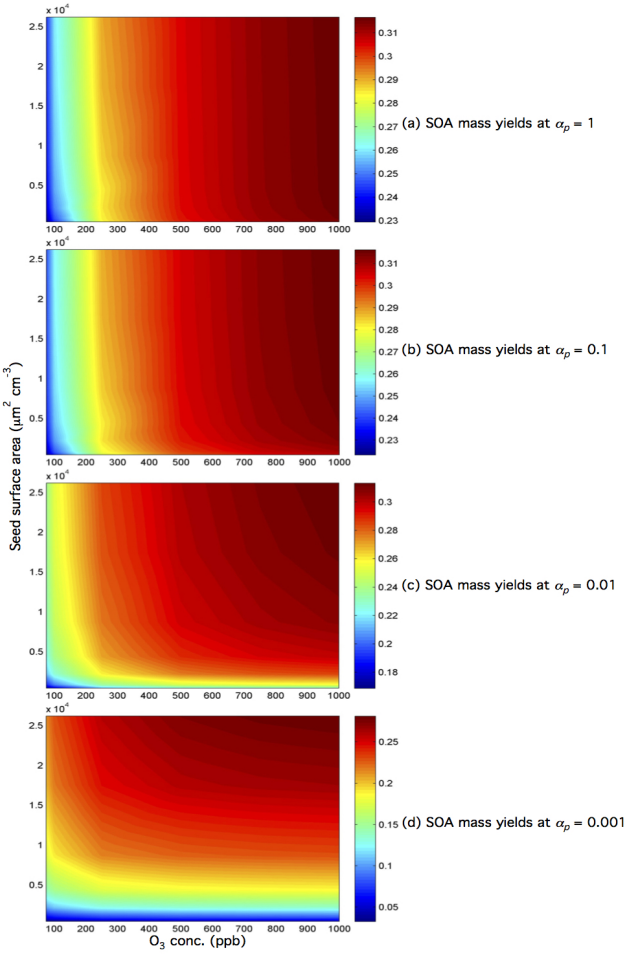

Figure 6. SOA mass yields at peak SOA growth as a function of both the seed surface area and O_3 concentration for $\alpha_p = 1$, 0.1, 0.01, and 0.001. The SOA mass yields at peak SOA growth are indicated by colors and contours. Note that the color bars for panels **(a, b, c)** have different SOA mass yield ranges. Simulations were carried out using the optimal branching ratios, oligomerization rate, and vapor wall deposition rate parameters obtained in this study. The initial α-pinene concentration was set to 50 ppb, and a fixed O_3 concentration was used in place of a linear injection.

when higher seed aerosol number concentrations (relative to those used in this study) are used (Seinfeld and Pandis, 2006; Pierce et al., 2008). A detailed analysis of the effect of seed aerosol surface area concentrations $> 3000\,\mu m^2\,cm^{-3}$ on α-pinene ozonolysis SOA mass yields will be the subject of forthcoming work.

Higher SOA mass yields at peak SOA growth are observed in the present study when O_3 is increased from 100 to 500 ppb. This is because α-pinene is oxidized more quickly, which leads to gas-phase oxidation products being formed more rapidly and consequently partitioning more quickly onto AS seed aerosol particles before they are lost to the chamber walls. Therefore, the oxidation rate effect (i.e., higher SOA mass yields as a result of faster hydrocarbon oxidation rates) is a consequence of vapor wall deposition. An important implication of this study is that SOA mass yields can be affected by vapor wall deposition in VOC systems that are not characterized by slow mass accommodation of gas-phase organics to the particle phase (Zhang et al., 2014). Thus, this work demonstrates that the effect of vapor wall deposition on SOA mass yields can be mitigated through the use of excess oxidant concentrations. It should be noted that the α-pinene ozonolysis SOA mass yields (absolute values) increased by 5 to 9 % when O_3 is increased from 100 to 500 ppb (for an initial α-pinene concentration of $\sim$ 50 ppb), where SOA formation is governed by quasi-equilibrium growth. In the absence of vapor wall deposition, SOA mass yields are predicted by the model used here to approximately double from those observed experimentally. In contrast, Zhang et al. (2014) showed that the presence of vapor wall deposition led to underestimation of SOA formation by factors as much as 4 in the toluene photooxidation system, where the condensation of SOA-forming vapors onto seed aerosol is kinetically limited. Taken together, these results indicate that the magnitude by which vapor wall deposition affects SOA mass yields depends on the extent to which the VOC system is governed by kinetically limited SOA condensational growth.

Given these observations of how gas–particle partitioning can influence the magnitude by which vapor wall deposition affects SOA mass yields, an overriding question is, what controls the gas–particle partitioning behavior of SOA formed in different VOC systems? α_p describes the overall mass transfer of vapor molecules into the particle phase (McVay et al., 2014; Zhang et al., 2014). Thus, α_p affects the vapor-particle equilibrium timescale, which, depending on the extent to which it is competitive with the timescales for reaction and vapor wall deposition, determines whether SOA formation is governed by kinetically limited or quasi-equilibrium growth. Markedly different $\alpha_p$values could arise from the physical phase state of the SOA formed. As discussed by McVay et al. (2014, 2016), if the SOA formed exists in a semi-solid state (Vaden et al., 2010, 2011; Virtanen et al., 2010, 2011; Cappa and Wilson, 2011; Kuwata and Martin, 2012; Perraud et al., 2012; Saukko et al., 2012; Abramson et al., 2013; Renbaum-Wolff et al., 2013), a low value of α_p might be expected owing to retarded surface accommodation and particle-phase diffusion (Zaveri et al., 2014). Quantification of α_p is challenging experimentally, and reported α_p values for the same system can vary by several orders of magnitude (Grieshop et al., 2007; Stanier et al., 2007; Vaden et al., 2011; Miles et al., 2012; Saleh et al., 2013; Saha and Grieshop, 2016). Therefore, α_p of SOA formed in different VOC systems needs to be better constrained through a combination of experimental and modeling efforts.

While not investigated in detail in this study, the timescale of oligomerization may play an important role depending on the SOA growth regime (i.e., kinetically limited vs. quasi-

Table 2. Coupled vapor–particle dynamics model parameters.

Parameter	Definition	Value
α_p	Vapor–particle mass accommodation coefficient	0.1
α_w	Vapor–wall mass accommodation coefficient	10^{-6}
τ_{olig}	Timescale of oligomerization	4 h
C^*	Branching ratios and saturation concentrations of oxidation products	[0.6 ($>10^3$), 0.3(10^2), 0.05(10), 0.05(1) and 0(0.1)]
D_i	Gas-phase molecular diffusivity	3×10^{-6} m^2 s^{-1}
A/V	Surface area-to-volume ratio of the chamber	2.5 m^{-1}
C_w	Equivalent organic mass concentration in the wall	10 mg m^{-3}
k_e	Eddy diffusion coefficient	0.03 s^{-1}
M_i	Molecular weight of the diffusing gas-phase molecule i	168, 184, 192, 200 and 216 g mol^{-1}
M_{init}	Initially absorbing organic material in seed aerosol	0.01 µg m^{-3}
P	Pressure	1×10^5 Pa
T	Temperature	298 K
ρ_{seed}	Density of inorganic seed	1700 kg m^{-3}
ρ_{org}	Density of organic material on seed particle	1300 kg m^{-3}

equilibrium). Currently, it is unclear how the timescale of oligomerization in a VOC system where SOA formation is dominated by quasi-equilibrium growth (e.g., α-pinene ozonolysis) may differ from one that is dominated by kinetically limited growth (e.g., toluene photooxidation; Zhang et al., 2014). This requires further investigation through a combination of experimental and modeling efforts to improve our understanding of how particle-phase processes (e.g., oligomerization) affect gas–particle partitioning and consequently influence the magnitude by which vapor wall deposition affects SOA mass yields.

The SOA mass yield from the ozonolysis of monoterpenes in the GEOS-CHEM chemical transport model (19 % at 10 µg m^{-3}) is currently based on that measured in α-pinene ozonolysis studies by Shilling et al. (2008) (Pye et al., 2010). Shilling et al. (2008) measured these SOA mass yields in a Teflon chamber operated in continuous-flow mode, as opposed to batch mode, which is how experiments in the present study and most of those shown in Fig. 5 and Table S3 were conducted. While it is not possible to directly compare our results with those of Shilling et al. (2008) due to differences in SOA mass concentrations, the SOA mass concentrations and yields measured in the current study are generally consistent with those of previous batch chamber studies. The SOA mass yields at $\sim$ 10 µg m^{-3} SOA mass concentration measured by Shilling et al. (2008) are generally higher than those measured in chambers operated in batch mode (Griffin et al., 1999; Cocker et al., 2001b; Presto et al., 2005; Presto and Donahue, 2006; Pathak et al., 2007b) (Fig. 5). One possible explanation for the higher SOA mass yields in the continuous-flow, steady-state mode is that the SOA-forming vapors are in equilibrium with the chamber walls and seed aerosol, hence minimizing the irreversible loss of SOA-forming vapors to the chamber walls (Shilling et al., 2008). However, the extent to which SOA mass yields obtained in a continuous-flow reactor are influenced by vapor wall loss is unclear. Using a continuous-flow reactor, Ehn et al. (2014) observed α-pinene ozonolysis SOA mass yields to increase with increasing seed aerosol surface area but required $\alpha_p = 1$ to fit the observed SOA growth. The observed vapor wall deposition rate constant in their continuous-flow reactor (0.011 s^{-1}) is 2 orders of magnitude larger than that of the GTEC chamber (10^{-4} s^{-1}). The estimated timescales for gas–particle and gas–wall partitioning are also approximately equal in their continuous-flow reactor. This indicates that SOA condensational growth is kinetically limited in their continuous-flow reactor even at $\alpha_p = 1$ (Ehn et al., 2014; McVay et al., 2014), which suggests that SOA mass yields measured in their continuous-flow reactor may be significantly affected by vapor wall deposition.

Previous studies on SOA formation from the OH and NO_3 oxidation of biogenic VOCs have similarly reported higher SOA mass yields in the presence of higher oxidant concentrations. For example, in the NO_3 oxidation of β-pinene, Boyd et al. (2015) reported SOA mass yields 10 to 30 % higher than those previously reported by Fry et al. (2009, 2014). In addition to differences in the experimental conditions of the two studies (which may lead to differing RO_2 chemistry), Boyd et al. (2015) hypothesized that the higher SOA mass yields could also be a result of the higher NO_3 concentrations used in their study (which led to faster β-pinene oxidation rates) compared to those used by Fry et al. (2009, 2014). The oxidation rate effect was also observed in the m-xylene photooxidation system, where Ng et al. (2007) showed that the SOA mass yields were dependent on the m-xylene oxidation rate, with higher OH concentrations (and hence faster oxidation rates) resulting in higher SOA mass yields. The authors dismissed the possibility of the different SOA mass yields being a result of different RO_2 chemistry since all their m-xylene photooxidation experiments were performed under high-NO_x conditions and the RO_2 reacted virtually entirely with NO. Together, these studies show that faster hydrocar-

bon oxidation rates can alleviate the effects of vapor wall deposition on SOA mass yields in different VOC systems.

This gives rise to the question of whether chamber SOA experiments on different VOC systems should be performed under as rapid oxidation conditions as possible (i.e., large oxidant concentrations) to reduce the effects of vapor wall deposition. A recent study by McVay et al. (2016) reported similar SOA growth under low and high OH levels for α-pinene photooxidation. The authors hypothesized that the autoxidation mechanism likely becomes a more important pathway at low OH levels (Crounse et al., 2013) and thus contributes substantially to SOA growth. Therefore, it is possible that certain reaction pathways and mechanisms (which are important in the atmosphere) are biased when unusually high levels of oxidants are used in chamber experiments (e.g., autoxidation). Thus, this underscores the need to design chamber experiments that simultaneously mitigate the magnitude of vapor wall deposition while ensuring that reaction conditions, and consequently reaction pathways and oxidation products, are atmospherically relevant. More importantly, the impact of vapor wall deposition on SOA formation and evolution in various VOC systems conducted under different reaction conditions (regardless of atmospheric relevance) needs to be quantified through a combination of experimental and modeling efforts. Similar to this study, experiments should be performed using different seed aerosol surface area and oxidant concentrations to study their influence on vapor wall deposition and SOA mass yields. If the effects of vapor wall loss are found to be strongly dependent on seed aerosol surface area and/or oxidant concentrations (e.g., toluene photooxidation, where SOA formation may be underestimated by factors as much as 4; Zhang et al., 2014), further experiments aimed at measuring the wall deposition rates of the oxidation products should be performed. These wall deposition rates can then be used in predictive models to determine the vapor–wall and vapor–particle mass accommodation coefficients of these oxidation products. Consequently, this will allow us to determine the fraction of SOA-forming vapors partitioning to the particle phase vs. lost to the chamber walls (Zhang et al., 2015a; Krechmer et al., 2016).

7 Data availability

The experimental data and model output can be accessed by request (ng@chbe.gatech.edu).

The Supplement related to this article is available online at doi:10.5194/acp-16-9361-2016-supplement.

Acknowledgements. This research was funded by NSF grants 1455588 and AGS-1523500, and US Environmental Protection Agency STAR grant (Early Career) RD-83540301. This publication's contents are solely the responsibility of the grantee and do not necessarily represent the official views of the US EPA. Further, US EPA does not endorse the purchase of any commercial products or services mentioned in the publication. R.C. McVay was supported by a National Science Foundation Graduate Research Fellowship under grant no. DGE-1144469.

Edited by: M. Shiraiwa
Reviewed by: two anonymous referees

References

Abramson, E., Imre, D., Beranek, J., Wilson, J., and Zelenyuk, A.: Experimental determination of chemical diffusion within secondary organic aerosol particles, Phys. Chem. Chem. Phys., 15, 2983–2991, doi:10.1039/c2cp44013j, 2013.

Bahreini, R., Keywood, M. D., Ng, N. L., Varutbangkul, V., Gao, S., Flagan, R. C., Seinfeld, J. H., Worsnop, D. R., and Jimenez, J. L.: Measurements of Secondary Organic Aerosol from Oxidation of Cycloalkenes, Terpenes, and m-Xylene Using an Aerodyne Aerosol Mass Spectrometer, Environ. Sci. Technol., 39, 5674–5688, doi:10.1021/es048061a, 2005.

Boyd, C. M., Sanchez, J., Xu, L., Eugene, A. J., Nah, T., Tuet, W. Y., Guzman, M. I., and Ng, N. L.: Secondary organic aerosol formation from the β-pinene + NO_3 system: effect of humidity and peroxy radical fate, Atmos. Chem. Phys., 15, 7497–7522, doi:10.5194/acp-15-7497-2015, 2015.

Canagaratna, M. R., Jimenez, J. L., Kroll, J. H., Chen, Q., Kessler, S. H., Massoli, P., Hildebrandt Ruiz, L., Fortner, E., Williams, L. R., Wilson, K. R., Surratt, J. D., Donahue, N. M., Jayne, J. T., and Worsnop, D. R.: Elemental ratio measurements of organic compounds using aerosol mass spectrometry: characterization, improved calibration, and implications, Atmos. Chem. Phys., 15, 253–272, doi:10.5194/acp-15-253-2015, 2015.

Capouet, M., Müller, J. F., Ceulemans, K., Compernolle, S., Vereecken, L., and Peeters, J.: Modeling aerosol formation in alpha-pinene photo-oxidation experiments, J. Geophys. Res.-Atmos., 113, D02308, doi:10.1029/2007JD008995, 2008.

Cappa, C. D. and Wilson, K. R.: Evolution of organic aerosol mass spectra upon heating: implications for OA phase and partitioning behavior, Atmos. Chem. Phys., 11, 1895–1911, doi:10.5194/acp-11-1895-2011, 2011.

Cappa, C. D., Jathar, S. H., Kleeman, M. J., Docherty, K. S., Jimenez, J. L., Seinfeld, J. H., and Wexler, A. S.: Simulating secondary organic aerosol in a regional air quality model using the statistical oxidation model – Part 2: Assessing the influence of vapor wall losses, Atmos. Chem. Phys., 16, 3041–3059, doi:10.5194/acp-16-3041-2016, 2016.

Carlton, A. G., Bhave, P. V., Napelenok, S. L., Edney, E. D., Sarwar, G., Pinder, R. W., Pouliot, G. A., and Houyoux, M.: Model Representation of Secondary Organic Aerosol in CMAQv4.7, Environ. Sci. Technol., 44, 8553–8560, doi:10.1021/es100636q, 2010.

Chan, A. W. H., Kroll, J. H., Ng, N. L., and Seinfeld, J. H.: Kinetic modeling of secondary organic aerosol formation: effects

of particle- and gas-phase reactions of semivolatile products, Atmos. Chem. Phys., 7, 4135–4147, doi:10.5194/acp-7-4135-2007, 2007.

Cocker, D. R., Flagan, R. C., and Seinfeld, J. H.: State-of-the-art chamber facility for studying atmospheric aerosol chemistry, Environ. Sci. Technol., 35, 2594–2601, doi:10.1021/es0019169, 2001a.

Cocker, D. R., Clegg, S. L., Flagan, R. C., and Seinfeld, J. H.: The effect of water on gas-particle partitioning of secondary organic aerosol. Part I: alpha-pinene/ozone system, Atmos. Environ., 35, 6049–6072, doi:10.1016/s1352-2310(01)00404-6, 2001b.

Crounse, J. D., Nielsen, L. B., Jorgensen, S., Kjaergaard, H. G., and Wennberg, P. O.: Autoxidation of Organic Compounds in the Atmosphere, J. Phys. Chem. Lett., 4, 3513–3520, 10.1021/jz4019207, 2013.

Crump, J. G. and Seinfeld, J. H.: Turbulent Deposition and Gravitational Sedimentation of an Aerosol in a Vessel of Arbitrary Shape, J. Aerosol Sci., 12, 405–415, doi:10.1016/0021-8502(81)90036-7, 1981.

DeCarlo, P. F., Slowik, J. G., Worsnop, D. R., Davidovits, P., and Jimenez, J. L.: Particle morphology and density characterization by combined mobility and aerodynamic diameter measurements. Part 1: Theory, Aerosol Sci. Tech., 38, 1185–1205, doi:10.1080/027868290903907, 2004.

DeCarlo, P. F., Kimmel, J. R., Trimborn, A., Northway, M. J., Jayne, J. T., Aiken, A. C., Gonin, M., Fuhrer, K., Horvath, T., Docherty, K. S., Worsnop, D. R., and Jimenez, J. L.: Field-deployable, high-resolution, time-of-flight aerosol mass spectrometer, Anal. Chem., 78, 8281–8289, doi:10.1021/ac061249n, 2006.

Docherty, K. S., Wu, W., Lim, Y. B., and Ziemann, P. J.: Contributions of organic peroxides to secondary aerosol formed from reactions of monoterpenes with O_3, Environ. Sci. Technol., 39, 4049–4059, doi:10.1021/es050228s, 2005.

Donahue, N. M., Robinson, A. L., Stanier, C. O., and Pandis, S. N.: Coupled partitioning, dilution, and chemical aging of semivolatile organics, Environ. Sci. Technol., 40, 2635–2643, doi:10.1021/es052297c, 2006.

Donahue, N. M., Epstein, S. A., Pandis, S. N., and Robinson, A. L.: A two-dimensional volatility basis set: 1. organic-aerosol mixing thermodynamics, Atmos. Chem. Phys., 11, 3303–3318, doi:10.5194/acp-11-3303-2011, 2011.

Ehn, M., Thornton, J. A., Kleist, E., Sipila, M., Junninen, H., Pullinen, I., Springer, M., Rubach, F., Tillmann, R., Lee, B., Lopez-Hilfiker, F., Andres, S., Acir, I. H., Rissanen, M., Jokinen, T., Schobesberger, S., Kangasluoma, J., Kontkanen, J., Nieminen, T., Kurten, T., Nielsen, L. B., Jorgensen, S., Kjaergaard, H. G., Canagaratna, M., Dal Maso, M., Berndt, T., Petaja, T., Wahner, A., Kerminen, V. M., Kulmala, M., Worsnop, D. R., Wildt, J., and Mentel, T. F.: A large source of low-volatility secondary organic aerosol, Nature, 506, 476–479, doi:10.1038/nature13032, 2014.

Fry, J. L., Kiendler-Scharr, A., Rollins, A. W., Wooldridge, P. J., Brown, S. S., Fuchs, H., Dubé, W., Mensah, A., dal Maso, M., Tillmann, R., Dorn, H.-P., Brauers, T., and Cohen, R. C.: Organic nitrate and secondary organic aerosol yield from NO_3 oxidation of β-pinene evaluated using a gas-phase kinetics/aerosol partitioning model, Atmos. Chem. Phys., 9, 1431–1449, doi:10.5194/acp-9-1431-2009, 2009.

Fry, J. L., Draper, D. C., Barsanti, K. C., Smith, J. N., Ortega, J., Winkler, P. M., Lawler, M. J., Brown, S. S., Edwards, P. M., Cohen, R. C., and Lee, L.: Secondary Organic Aerosol Formation and Organic Nitrate Yield from NO_3 Oxidation of Biogenic Hydrocarbons, Environ. Sci. Technol., 48, 11944–11953, doi:10.1021/es502204x, 2014.

Gao, S., Ng, N. L., Keywood, M., Varutbangkul, V., Bahreini, R., Nenes, A., He, J. W., Yoo, K. Y., Beauchamp, J. L., Hodyss, R. P., Flagan, R. C., and Seinfeld, J. H.: Particle phase acidity and oligomer formation in secondary organic aerosol, Environ. Sci. Technol., 38, 6582–6589, doi:10.1021/es049125k, 2004.

Grieshop, A. P., Donahue, N. M., and Robinson, A. L.: Is the gas-particle partitioning in alpha-pinene secondary organic aerosol reversible?, Geophys. Res. Lett., 34, L14810, doi:10.1029/2007GL029987, 2007.

Griffin, R. J., Cocker, D. R., Flagan, R. C., and Seinfeld, J. H.: Organic aerosol formation from the oxidation of biogenic hydrocarbons, J. Geophys. Res.-Atmos., 104, 3555–3567, doi:10.1029/1998jd100049, 1999.

Guenther, A. B., Jiang, X., Heald, C. L., Sakulyanontvittaya, T., Duhl, T., Emmons, L. K., and Wang, X.: The Model of Emissions of Gases and Aerosols from Nature version 2.1 (MEGAN2.1): an extended and updated framework for modeling biogenic emissions, Geosci. Model Dev., 5, 1471–1492, doi:10.5194/gmd-5-1471-2012, 2012.

Hallquist, M., Wenger, J. C., Baltensperger, U., Rudich, Y., Simpson, D., Claeys, M., Dommen, J., Donahue, N. M., George, C., Goldstein, A. H., Hamilton, J. F., Herrmann, H., Hoffmann, T., Iinuma, Y., Jang, M., Jenkin, M. E., Jimenez, J. L., Kiendler-Scharr, A., Maenhaut, W., McFiggans, G., Mentel, Th. F., Monod, A., Prévôt, A. S. H., Seinfeld, J. H., Surratt, J. D., Szmigielski, R., and Wildt, J.: The formation, properties and impact of secondary organic aerosol: current and emerging issues, Atmos. Chem. Phys., 9, 5155–5236, doi:10.5194/acp-9-5155-2009, 2009.

Henry, K. M., Lohaus, T., and Donahue, N. M.: Organic Aerosol Yields from alpha-Pinene Oxidation: Bridging the Gap between First-Generation Yields and Aging Chemistry, Environ. Sci. Technol., 46, 12347–12354, doi:10.1021/es302060y, 2012.

Hildebrandt, L., Donahue, N. M., and Pandis, S. N.: High formation of secondary organic aerosol from the photo-oxidation of toluene, Atmos. Chem. Phys., 9, 2973–2986, doi:10.5194/acp-9-2973-2009, 2009.

Hoffmann, T., Odum, J. R., Bowman, F., Collins, D., Klockow, D., Flagan, R. C., and Seinfeld, J. H.: Formation of organic aerosols from the oxidation of biogenic hydrocarbons, J. Atmos. Chem., 26, 189–222, doi:10.1023/a:1005734301837, 1997.

Kanakidou, M., Seinfeld, J. H., Pandis, S. N., Barnes, I., Dentener, F. J., Facchini, M. C., Van Dingenen, R., Ervens, B., Nenes, A., Nielsen, C. J., Swietlicki, E., Putaud, J. P., Balkanski, Y., Fuzzi, S., Horth, J., Moortgat, G. K., Winterhalter, R., Myhre, C. E. L., Tsigaridis, K., Vignati, E., Stephanou, E. G., and Wilson, J.: Organic aerosol and global climate modelling: a review, Atmos. Chem. Phys., 5, 1053–1123, doi:10.5194/acp-5-1053-2005, 2005.

Karnezi, E., Riipinen, I., and Pandis, S. N.: Measuring the atmospheric organic aerosol volatility distribution: a theoretical analysis, Atmos. Meas. Tech., 7, 2953–2965, doi:10.5194/amt-7-2953-2014, 2014.

Keywood, M. D., Varutbangkul, V., Bahreini, R., Flagan, R. C., and Seinfeld, J. H.: Secondary organic aerosol formation from the

ozonolysis of cycloalkenes and related compounds, Environ. Sci. Technol., 38, 4157–4164, doi:10.1021/es035363o, 2004.

Kokkola, H., Yli-Pirilä, P., Vesterinen, M., Korhonen, H., Keskinen, H., Romakkaniemi, S., Hao, L., Kortelainen, A., Joutsensaari, J., Worsnop, D. R., Virtanen, A., and Lehtinen, K. E. J.: The role of low volatile organics on secondary organic aerosol formation, Atmos. Chem. Phys., 14, 1689–1700, doi:10.5194/acp-14-1689-2014, 2014.

Kostenidou, E., Pathak, R. K., and Pandis, S. N.: An algorithm for the calculation of secondary organic aerosol density combining AMS and SMPS data, Aerosol Sci. Tech., 41, 1002–1010, doi:10.1080/02786820701666270, 2007.

Krechmer, J. E., Pagonis, D., Ziemann, P. J., and Jimenez, J. L.: Quantification of Gas-Wall Partitioning in Teflon Environmental Chambers Using Rapid Bursts of Low-Volatility Oxidized Species Generated in Situ, Environ. Sci. Technol., 50, 5757–5765, doi:10.1021/acs.est.6b00606, 2016.

Kristensen, K., Cui, T., Zhang, H., Gold, A., Glasius, M., and Surratt, J. D.: Dimers in α-pinene secondary organic aerosol: effect of hydroxyl radical, ozone, relative humidity and aerosol acidity, Atmos. Chem. Phys., 14, 4201–4218, doi:10.5194/acp-14-4201-2014, 2014.

Kroll, J. H., Chan, A. W. H., Ng, N. L., Flagan, R. C., and Seinfeld, J. H.: Reactions of semivolatile organics and their effects on secondary organic aerosol formation, Environ. Sci. Technol., 41, 3545–3550, doi:10.1021/es062059x, 2007.

Kuwata, M. and Martin, S. T.: Phase of atmospheric secondary organic material affects its reactivity, P. Natl. Acad. Sci. USA, 109, 17354–17359, doi:10.1073/pnas.1209071109, 2012.

La, Y. S., Camredon, M., Ziemann, P. J., Valorso, R., Matsunaga, A., Lannuque, V., Lee-Taylor, J., Hodzic, A., Madronich, S., and Aumont, B.: Impact of chamber wall loss of gaseous organic compounds on secondary organic aerosol formation: explicit modeling of SOA formation from alkane and alkene oxidation, Atmos. Chem. Phys., 16, 1417–1431, doi:10.5194/acp-16-1417-2016, 2016.

Loza, C. L., Chan, A. W. H., Galloway, M. M., Keutsch, F. N., Flagan, R. C., and Seinfeld, J. H.: Characterization of Vapor Wall Loss in Laboratory Chambers, Environ. Sci. Technol., 44, 5074–5078, doi:10.1021/es100727v, 2010.

Loza, C. L., Chhabra, P. S., Yee, L. D., Craven, J. S., Flagan, R. C., and Seinfeld, J. H.: Chemical aging of *m*-xylene secondary organic aerosol: laboratory chamber study, Atmos. Chem. Phys., 12, 151–167, doi:10.5194/acp-12-151-2012, 2012.

Matsunaga, A. and Ziemann, P. J.: Gas-Wall Partitioning of Organic Compounds in a Teflon Film Chamber and Potential Effects on Reaction Product and Aerosol Yield Measurements, Aerosol Sci. Tech., 44, 881–892, doi:10.1080/02786826.2010.501044, 2010.

McMurry, P. H. and Grosjean, D.: Gas and Aerosol Wall Losses in Teflon Film Smog Chambers, Environ. Sci. Technol., 19, 1176–1182, doi:10.1021/es00142a006, 1985.

McMurry, P. H. and Rader, D. J.: Aerosol Wall Losses in Electrically Charged Chambers, Aerosol Sci. Tech., 4, 249–268, doi:10.1080/02786828508959054, 1985.

McVay, R. C., Cappa, C. D., and Seinfeld, J. H.: Vapor-Wall Deposition in Chambers: Theoretical Considerations, Environ. Sci. Technol., 48, 10251–10258, doi:10.1021/es502170j, 2014.

McVay, R. C., Zhang, X., Aumont, B., Valorso, R., Camredon, M., La, Y. S., Wennberg, P. O., and Seinfeld, J. H.: SOA formation from the photooxidation of α-pinene: systematic exploration of the simulation of chamber data, Atmos. Chem. Phys., 16, 2785–2802, doi:10.5194/acp-16-2785-2016, 2016.

Miles, R. E. H., Reid, J. P., and Riipinen, I.: Comparison of Approaches for Measuring the Mass Accommodation Coefficient for the Condensation of Water and Sensitivities to Uncertainties in Thermophysical Properties, J. Phys. Chem. A, 116, 10810–10825, doi:10.1021/jp3083858, 2012.

Ng, N. L., Kroll, J. H., Keywood, M. D., Bahreini, R., Varutbangkul, V., Flagan, R. C., Seinfeld, J. H., Lee, A., and Goldstein, A. H.: Contribution of first- versus second-generation products to secondary organic aerosols formed in the oxidation of biogenic hydrocarbons, Environ. Sci. Technol., 40, 2283–2297, doi:10.1021/es052269u, 2006.

Ng, N. L., Kroll, J. H., Chan, A. W. H., Chhabra, P. S., Flagan, R. C., and Seinfeld, J. H.: Secondary organic aerosol formation from *m*-xylene, toluene, and benzene, Atmos. Chem. Phys., 7, 3909–3922, doi:10.5194/acp-7-3909-2007, 2007.

Odum, J. R., Hoffmann, T., Bowman, F., Collins, D., Flagan, R. C., and Seinfeld, J. H.: Gas/Particle Partitioning and Secondary Organic Aerosol Yields, Environ. Sci. Technol., 30, 2580–2585, doi:10.1021/es950943+, 1996.

Odum, J. R., Jungkamp, T. P. W., Griffin, R. J., Flagan, R. C., and Seinfeld, J. H.: The atmospheric aerosol-forming potential of whole gasoline vapor, Science, 276, 96–99, doi:10.1126/science.276.5309.96, 1997a.

Odum, J. R., Jungkamp, T. P. W., Griffin, R. J., Forstner, H. J. L., Flagan, R. C., and Seinfeld, J. H.: Aromatics, reformulated gasoline, and atmospheric organic aerosol formation, Environ. Sci. Technol., 31, 1890–1897, doi:10.1021/es960535l, 1997b.

Pathak, R. K., Presto, A. A., Lane, T. E., Stanier, C. O., Donahue, N. M., and Pandis, S. N.: Ozonolysis of α-pinene: parameterization of secondary organic aerosol mass fraction, Atmos. Chem. Phys., 7, 3811–3821, doi:10.5194/acp-7-3811-2007, 2007a.

Pathak, R. K., Stanier, C. O., Donahue, N. M., and Pandis, S. N.: Ozonolysis of alpha-pinene at atmospherically relevant concentrations: Temperature dependence of aerosol mass fractions (yields), J. Geophys. Res.-Atmos., 112, D03201, doi:10.1029/2006jd007436, 2007b.

Perraud, V., Bruns, E. A., Ezell, M. J., Johnson, S. N., Yu, Y., Alexander, M. L., Zelenyuk, A., Imre, D., Chang, W. L., Dabdub, D., Pankow, J. F., and Finlayson-Pitts, B. J.: Nonequilibrium atmospheric secondary organic aerosol formation and growth, P. Natl. Acad. Sci. USA, 109, 2836–2841, doi:10.1073/pnas.1119909109, 2012.

Pierce, J. R., Engelhart, G. J., Hildebrandt, L., Weitkamp, E. A., Pathak, R. K., Donahue, N. M., Robinson, A. L., Adams, P. J., and Pandis, S. N.: Constraining particle evolution from wall losses, coagulation, and condensation-evaporation in smog-chamber experiments: Optimal estimation based on size distribution measurements, Aerosol Sci. Tech., 42, 1001–1015, doi:10.1080/02786820802389251, 2008.

Presto, A. A. and Donahue, N. M.: Investigation of alpha-pinene plus ozone secondary organic aerosol formation at low total aerosol mass, Environ. Sci. Technol., 40, 3536–3543, doi:10.1021/es052203z, 2006.

Presto, A. A., Hartz, K. E. H., and Donahue, N. M.: Secondary organic aerosol production from terpene ozonolysis. 2. Effect

of NO_x concentration, Environ. Sci. Technol., 39, 7046–7054, doi:10.1021/es050400s, 2005.

Pye, H. O. T., Chan, A. W. H., Barkley, M. P., and Seinfeld, J. H.: Global modeling of organic aerosol: the importance of reactive nitrogen (NO_x and NO_3), Atmos. Chem. Phys., 10, 11261–11276, doi:10.5194/acp-10-11261-2010, 2010.

Renbaum-Wolff, L., Grayson, J. W., Bateman, A. P., Kuwata, M., Sellier, M., Murray, B. J., Shilling, J. E., Martin, S. T., and Bertram, A. K.: Viscosity of alpha-pinene secondary organic material and implications for particle growth and reactivity, P. Natl. Acad. Sci. USA, 110, 8014–8019, doi:10.1073/pnas.1219548110, 2013.

Saha, P. K. and Grieshop, A. P.: Exploring Divergent Volatility Properties from Yield and Thermodenuder Measurements of Secondary Organic Aerosol from α-Pinene Ozonolysis, Environ. Sci. Technol., 50, 5740–5749, doi:10.1021/acs.est.6b00303, 2016.

Saleh, R., Donahue, N. M., and Robinson, A. L.: Time Scales for Gas-Particle Partitioning Equilibration of Secondary Organic Aerosol Formed from Alpha-Pinene Ozonolysis, Environ. Sci. Technol., 47, 5588–5594, doi:10.1021/es400078d, 2013.

Saukko, E., Lambe, A. T., Massoli, P., Koop, T., Wright, J. P., Croasdale, D. R., Pedernera, D. A., Onasch, T. B., Laaksonen, A., Davidovits, P., Worsnop, D. R., and Virtanen, A.: Humidity-dependent phase state of SOA particles from biogenic and anthropogenic precursors, Atmos. Chem. Phys., 12, 7517–7529, doi:10.5194/acp-12-7517-2012, 2012.

Saunders, S. M., Jenkin, M. E., Derwent, R. G., and Pilling, M. J.: Protocol for the development of the Master Chemical Mechanism, MCM v3 (Part A): tropospheric degradation of non-aromatic volatile organic compounds, Atmos. Chem. Phys., 3, 161–180, doi:10.5194/acp-3-161-2003, 2003.

Seinfeld, J. H. and Pandis, S. N.: Atmospheric chemistry and physics: from air pollution to climate change, 2nd Edn., Wiley, Hoboken, N.J., xxviii, 1203 pp., 2006.

Shilling, J. E., Chen, Q., King, S. M., Rosenoern, T., Kroll, J. H., Worsnop, D. R., McKinney, K. A., and Martin, S. T.: Particle mass yield in secondary organic aerosol formed by the dark ozonolysis of α-pinene, Atmos. Chem. Phys., 8, 2073–2088, doi:10.5194/acp-8-2073-2008, 2008.

Shilling, J. E., Chen, Q., King, S. M., Rosenoern, T., Kroll, J. H., Worsnop, D. R., DeCarlo, P. F., Aiken, A. C., Sueper, D., Jimenez, J. L., and Martin, S. T.: Loading-dependent elemental composition of α-pinene SOA particles, Atmos. Chem. Phys., 9, 771–782, doi:10.5194/acp-9-771-2009, 2009.

Shiraiwa, M. and Seinfeld, J. H.: Equilibration timescale of atmospheric secondary organic aerosol partitioning, Geophys. Res. Lett., 39, L24801, doi:10.1029/2012gl054008, 2012.

Song, C., Zaveri, R. A., Alexander, M. L., Thornton, J. A., Madronich, S., Ortega, J. V., Zelenyuk, A., Yu, X. Y., Laskin, A., and Maughan, D. A.: Effect of hydrophobic primary organic aerosols on secondary organic aerosol formation from ozonolysis of alpha-pinene, Geophys. Res. Lett., 34, L20803, doi:10.1029/2007gl030720, 2007.

Stanier, C. O., Pathak, R. K., and Pandis, S. N.: Measurements of the volatility of aerosols from α-piniene ozonolysis, Environ. Sci. Technol., 41, 2756–2763, doi:10.1021/es0519280, 2007.

Tange, O.: GNU Parallel – The Command-Line Power Tool, :login: The USENIX Magazine, available at: http://www.gnu.org/s/parallel (last access: 15 June 2016), 2011.

Tsigaridis, K., Daskalakis, N., Kanakidou, M., Adams, P. J., Artaxo, P., Bahadur, R., Balkanski, Y., Bauer, S. E., Bellouin, N., Benedetti, A., Bergman, T., Berntsen, T. K., Beukes, J. P., Bian, H., Carslaw, K. S., Chin, M., Curci, G., Diehl, T., Easter, R. C., Ghan, S. J., Gong, S. L., Hodzic, A., Hoyle, C. R., Iversen, T., Jathar, S., Jimenez, J. L., Kaiser, J. W., Kirkevåg, A., Koch, D., Kokkola, H., Lee, Y. H., Lin, G., Liu, X., Luo, G., Ma, X., Mann, G. W., Mihalopoulos, N., Morcrette, J.-J., Müller, J.-F., Myhre, G., Myriokefalitakis, S., Ng, N. L., O'Donnell, D., Penner, J. E., Pozzoli, L., Pringle, K. J., Russell, L. M., Schulz, M., Sciare, J., Seland, Ø., Shindell, D. T., Sillman, S., Skeie, R. B., Spracklen, D., Stavrakou, T., Steenrod, S. D., Takemura, T., Tiitta, P., Tilmes, S., Tost, H., van Noije, T., van Zyl, P. G., von Salzen, K., Yu, F., Wang, Z., Wang, Z., Zaveri, R. A., Zhang, H., Zhang, K., Zhang, Q., and Zhang, X.: The AeroCom evaluation and intercomparison of organic aerosol in global models, Atmos. Chem. Phys., 14, 10845–10895, doi:10.5194/acp-14-10845-2014, 2014.

Vaden, T. D., Song, C., Zaveri, R. A., Imre, D., and Zelenyuk, A.: Morphology of mixed primary and secondary organic particles and the adsorption of spectator organic gases during aerosol formation, P. Natl. Acad. Sci. USA, 107, 6658–6663, doi:10.1073/pnas.0911206107, 2010.

Vaden, T. D., Imre, D., Beranek, J., Shrivastava, M., and Zelenyuk, A.: Evaporation kinetics and phase of laboratory and ambient secondary organic aerosol, P. Natl. Acad. Sci. USA, 108, 2190–2195, doi:10.1073/pnas.1013391108, 2011.

Virtanen, A., Joutsensaari, J., Koop, T., Kannosto, J., Yli-Pirila, P., Leskinen, J., Makela, J. M., Holopainen, J. K., Pöschl, U., Kulmala, M., Worsnop, D. R., and Laaksonen, A.: An amorphous solid state of biogenic secondary organic aerosol particles, Nature, 467, 824–827, doi:10.1038/nature09455, 2010.

Virtanen, A., Kannosto, J., Kuuluvainen, H., Arffman, A., Joutsensaari, J., Saukko, E., Hao, L., Yli-Pirilä, P., Tiitta, P., Holopainen, J. K., Keskinen, J., Worsnop, D. R., Smith, J. N., and Laaksonen, A.: Bounce behavior of freshly nucleated biogenic secondary organic aerosol particles, Atmos. Chem. Phys., 11, 8759–8766, doi:10.5194/acp-11-8759-2011, 2011.

Weitkamp, E. A., Sage, A. M., Pierce, J. R., Donahue, N. M., and Robinson, A. L.: Organic aerosol formation from photochemical oxidation of diesel exhaust in a smog chamber, Environ. Sci. Technol., 41, 6969–6975, doi:10.1021/es070193r, 2007.

Ye, P., Ding, X., Hakala, J., Hofbauer, V., Robinson, E. S., and Donahue, N. M.: Vapor wall loss of semi-volatile organic compounds in a Teflon chamber, Aerosol Sci. Tech., 50, 822–834, doi:10.1080/02786826.2016.1195905, 2016.

Yeh, G. K. and Ziemann, P. J.: Alkyl Nitrate Formation from the Reactions of C-8-C-14 n-Alkanes with OH Radicals in the Presence of NO_x: Measured Yields with Essential Corrections for Gas-Wall Partitioning, J. Phys. Chem. A, 118, 8147–8157, doi:10.1021/jp500631v, 2014.

Yeh, G. K. and Ziemann, P. J.: Gas-Wall Partitioning of Oxygenated Organic Compounds: Measurements, Structure-Activity Relationships, and Correlation with Gas Chromatographic Retention Factor, Aerosol Sci. Tech., 49, 726–737, doi:10.1080/02786826.2015.1068427, 2015.

Zaveri, R. A., Easter, R. C., Shilling, J. E., and Seinfeld, J. H.: Modeling kinetic partitioning of secondary organic aerosol and size distribution dynamics: representing effects of volatility, phase state, and particle-phase reaction, Atmos. Chem. Phys., 14, 5153–5181, doi:10.5194/acp-14-5153-2014, 2014.

Zhang, X., Pandis, S. N., and Seinfeld, J. H.: Diffusion-Limited Versus Quasi-Equilibrium Aerosol Growth, Aerosol Sci. Tech., 46, 874–885, doi:10.1080/02786826.2012.679344, 2012.

Zhang, X., Cappa, C. D., Jathar, S. H., McVay, R. C., Ensberg, J. J., Kleeman, M. J., and Seinfeld, J. H.: Influence of vapor wall loss in laboratory chambers on yields of secondary organic aerosol, P. Natl. Acad. Sci. USA, 111, 5802–5807, doi:10.1073/pnas.1404727111, 2014.

Zhang, X., Schwantes, R. H., McVay, R. C., Lignell, H., Coggon, M. M., Flagan, R. C., and Seinfeld, J. H.: Vapor wall deposition in Teflon chambers, Atmos. Chem. Phys., 15, 4197–4214, doi:10.5194/acp-15-4197-2015, 2015a.

Zhang, X., McVay, R. C., Huang, D. D., Dalleska, N. F., Aumont, B., Flagan, R. C., and Seinfeld, J. H.: Formation and evolution of molecular products in alpha-pinene secondary organic aerosol, P. Natl. Acad. Sci. USA, 112, 14168–14173, doi:10.1073/pnas.1517742112, 2015b.